Master's thesis

Experimental study of quantum fluctuations in titanium nanowires in highly resistive environment

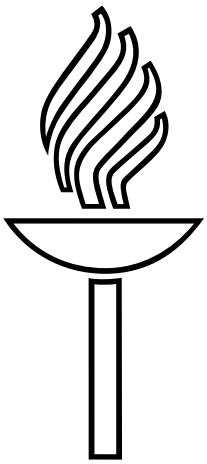

Janne Lehtinen

19.12.2009

UNIVERSITY OF JYVÄSKYLÄ
DEPARTMENT OF PHYSICS
NANOPHYSICS

Acknowledgements

The work covered in this thesis has been carried out at the Quantum nanoelectronics group in the University of Jyväskylä. The work was supervised by assistant professor Konstantin Arutyunov. I wish to give special thanks for the supervisor and Ms Terhi Hongisto who helped me with the low temperature measurements. I also want to thank everyone that have helped me in the project.

Jyväskylä 11.12.2009

Contents

Chapter 1

Introduction

Superconductivity was discovered by Kamerlingh Onnes in 1911 as he cooled down a mercury wire and found out that it lost all of its electrical resistivity. Nowadays the superconducting phenomina is already well known in the physics literature. The field is still all but throughoutly studied. Some intresting phenomina can only be measured in the nanoscale components. Also some challenging but very intresting materials are yet to be studied.

There are predictions and a limited number of experiments claiming mechanism of quantum phase tunneling. This effect exponentially depends on the cross section of a nanowire so far enabling its experimental observation in structures with the effective diameter $\sim$ 10 nm. The effect is of fundamental importance for our understanding of quantum coherent systems behavior in reduced dimensions. Titanium is a very promising material for the experimental proof of existence the quantum fluctuations. It as high resistivy companied by small T_c. This, according to the theoretical calculations, would allow observation of quantum fluctuations already at diameters of the nanowire around 30 nm.

Chapter 2

Objectives

The primary objective was to characterize electrical and physical properties of Ti-based nanowires and try to observe quantum fluctuations as the nanowire's dimensions are progressivily reduced by ion beam etching. The surface characterization of the nanostructures was done by SEM and AFM imaging. The electrical measurements were made in dilution refridgerator capable to reach temperature region around 60 $\pm$ 10 mK.

Secondary objective for the experiment was to fabricate a titanium nanowire in a highly resistive environment. This was done by utilizing angular evaporation of "dirty" titanium so that the superconductivity in the resistive probes was suppressed. The method appeared to be promising.

Chapter 3

Theoretical background

3.1 Microscopic characterization

The microscopic characterization of the samples was made with three different methods. The optical microscopy was used to get an image of the structure where the structure could be evaluated roughly. The optical microscopy is limited by wavelenght of the visible light but other factors also contribute to the resolution thus making the resulting resolution of sub-μm structures somewhat subjective. The numerical aperture, which consist of resolving power of an objective, numerical aperture of the substage condenser and wavelength of the illuminating light, determine specimen resolution. Also other factors, such as low specimen contrast and improper illumination may reduce the resolution. The magnification of the microscope doesn't affect the resolution. The best resolution attainable by optical microscopy is around 0.2 μm. An optical microscope image used the evaluate the structure taken with good quality optical microscope is presented in Figure 3.1.

Modern scanning electron microscope with a good secondary electron sensor is an effective tool for surface characterization. Even single metal grains of titanium with size of few nanometers are easily distinguishable in the images. The width of the wires and other parts of the structure can be measured with high accuracy (Figure 3.2). The continuity and the uniformity of the wires can be observed from the lower magnification images. The sample can be tilted for obtaining quasi-3-dimensional

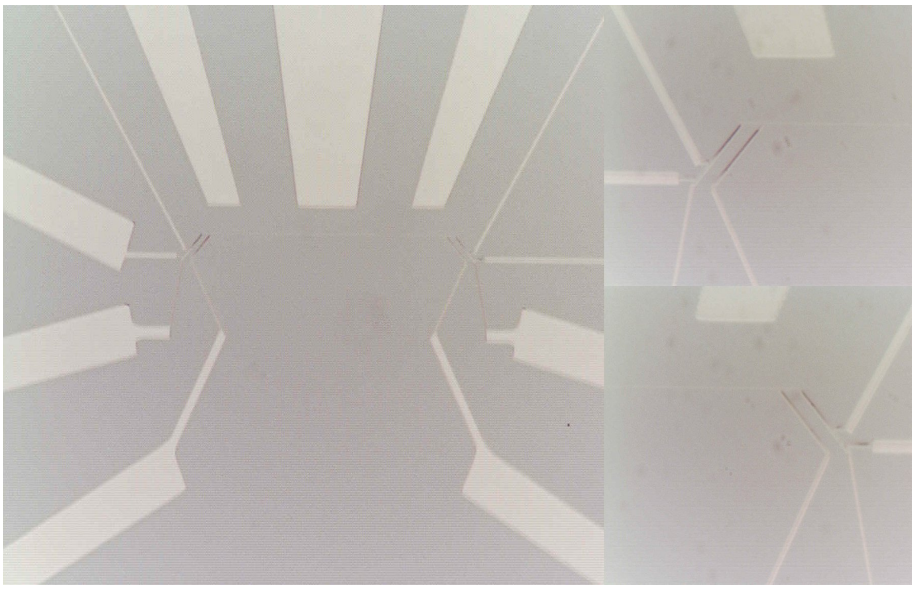

Figure 3.1: Good quality optical microscope images of a titanium nanowire and its contacts. The wire is about 50 nm wide and can be barely seen in the images.

images.

Atomic force microscopy is at its best when measuring the surface characteristics and the height of the sample(Figure 3.3). The wire heights and the the possible changes of the the crystal structure between sputtering steps were measured with AFM. The horizontal resolution of the AFM is not as good as in the SEM images. The resolution is limited by the step-size of the images and the radius of the tip. The vertical resolution of the AFM is very good and the height of the structures can be measured easily with $\sim$1 nm error.

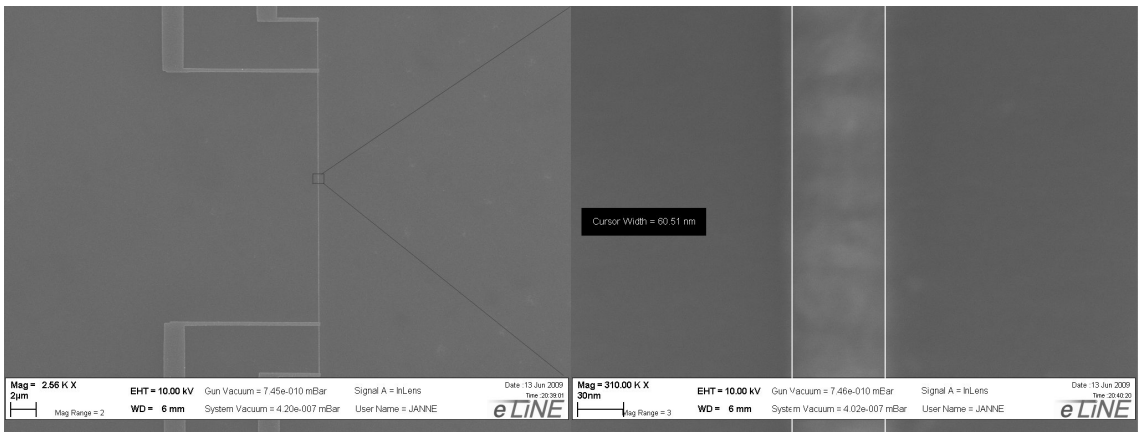

Figure 3.2: SEM image where the width of the nanowire is measured, normally the width is measured from multiple points.

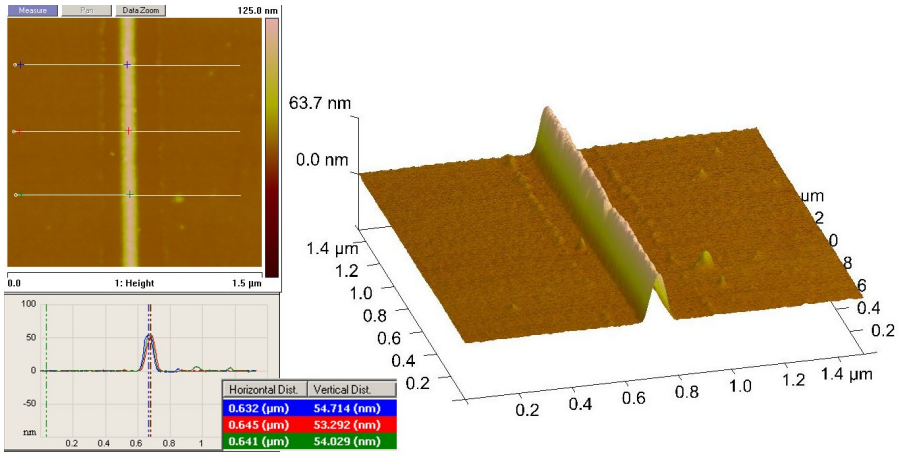

Figure 3.3: AFM image of a nanowire in 3D-presentation. The measurement of the height of the wire is done with three cross sections. The height is normally measured with the best possible accuracy which means that the amount of sections is limited by the step-size.

3.2 Theory of superconductivity

Superconductivity was discovered in 1911 by Kamerlingh Onnes. It took several decades untill a satisfactory explanation for the phenominon was made by J. Bardeen, L. N. Cooper and J. R. Schrieffer [1]. The finding of a new class of high T_C opened up a new chapter in physics of superconductivity in 1986 and revitalized the research. Though superconductivity has been known nearly hundred years, the field is still open for many areas of research, one of the most intresting beeing the nano-scale superconductivity. In this chapter the basic microscopic mechanism for classical superconductivity is explained.

3.2.1 Electron-phonon coupling

Weak attractions can bind electrons into electron pairs. In classical superconductivity this is attained by phonon-electron coupling. The electrons must over-come the residual screened inter-electron Coulomb repulsive interaction to achieve the supercondicting state.

The electron causes local polarization of a material by attracting positive ions in the vicinity. This leaves a distortion trail (Figure 3.4a). Such distortions have higher ion-density resulting an attractive influence to nearby electrons. This attraction is delayed by the difference of the time-scales of the electronic and ionic motion. The deformation is at the maximum when the average distance to the electron is approximately

$$d \approx \frac{v_F 2\pi}{\omega_D} \approx 100 - 300nm, \tag{3.1}$$

where v_F is the fermi velocity of the electron, typically (1 to 3)$*10^6 \frac{m}{s}$, and ω_D the Debye frequency which measures the response of the ionic sub-system and is about (2 to 8)$*10^{13} \frac{1}{s}$. The average electron pair separation is thus very large, of the scale of hundred nanometers and the Coulomb repulsion between the electrons is nearly totally screened.

The electron-phonon interaction is propably one of the easiest electron scattering

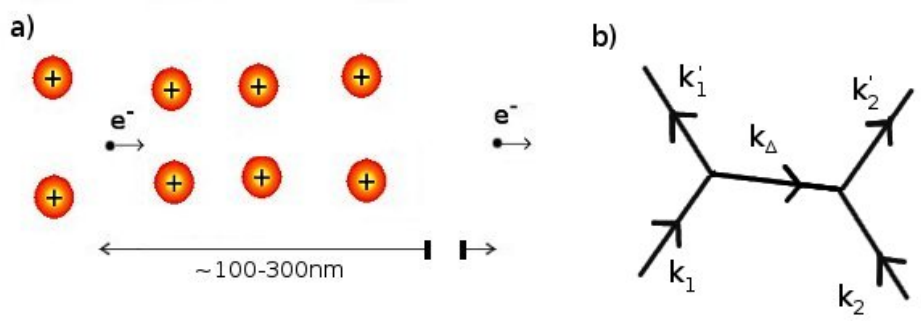

Figure 3.4: a) Electron - electron pairing by distortion trail within the ion lattice. b) Graphical representations of the electron-phonon scattering.

processes. An electron with state k_1 scatters to state $k_1^{'}$ by emiting a phonon with wavevector k_δ. A second electron can absorp the phonon and scatter from state k_2 to $k_2^{'}$. Conservation of the momemtum gives

$$k_1 - k_\Delta = k_1^{'} \tag{3.2}$$

$$k_2 + k_\Delta = k_2^{'} \tag{3.3}$$

$$k_1 + k_2 = k_1^{'} + k_2^{'} = k_0 \tag{3.4}$$

The process can be explaned by a qualitative picture of electron-phonon scattering (Figure 3.4b). Although the crystal momentum is conserved in each individual emission-scattering process, energy doesn't need to be conserved, and thus a virtual phonon can be emitted and absorbed within a very short time according to the Heisenberg's uncertainty relation.

The scattering events between two electrons require that the electrons occupy states $\epsilon > \epsilon_F$ at 0 K. The states that can interact are restricted by the Pauli exclusion principle to a shell of width δk corresponding electron energies between ϵ_F and $\epsilon_F + \hbar\omega_D$. Intersecting Fermi spheres separated by k_0 gives the allowed k-states involved in the scattering events. The number of such states is maximized when $k_0 = 0$ or $k_1 = -k_2$. Such pairs of electron are called Cooper pairs.

3.2.2 Cooper pairs

The electrons are fermions and obey the Pauli exclusion principle, but when paired – they behave more like bosons, which can condense into the same quantum state. In a general BCS-state, a finite fraction of electrons is bound into Cooper pairs and have the same state with respect to both relative and center-of-mass coordinate and thus the Cooper pairs are Bose-condensed.

The pair formalisms is adequate for classical superconductors(e.g. single element metals) and it propably includes also high-T_C superconductors with the exception that the pairing mechanism responsible for the Cooper pair formation in high-T_C superconductors is different.

To formulate the electron binding one should consider two electrons which are added to the Fermi a sea at T = 0 K. For simplicity the electrons interact only with each other and not with other electrons in the Fermi sea except via Pauli's exclusion principle. The lowest energy-state will be obtained when the particles have opposite momentum i.e. $k_1 = -k_2$. Thus we can write the two-particle equation as the product of the two plane-wave states

$$\Psi(r_1, r_2) = (\frac{1}{V^{\frac{1}{2}}} e^{ik\dot{r}_1})(\frac{1}{V^{\frac{1}{2}}} e^{-ik\dot{r}_2}) \tag{3.5}$$

A spherically symmetric wavefunction $\Psi(r_1, r_2) = \Psi(|r_1 - r_2|)$ means that the Cooper pair has no angular momentum, as is the case for the classical(s-wave) superconductors. Such equation is symmetric under the exchange of r_1 and r_2. By combining the symmetric spatial part with a spin wavefunction having an anti-symmetric combination of electron spins s_1 and s_2 we can obtain the total singlet-pair wavefunction

$$\Psi(1, 2) = \frac{\Psi(|r_1 - r_2|)(\alpha(1)\beta(2) - \alpha(2)\beta(1))}{\sqrt{2}} \tag{3.6}$$

The Cooper-pair in this equation is s-state paired (S = 0). This is the case in the conventional i.e. classical superconductor. Other combinations are still possible in the non-conventional superconductors. For spin-singlet case the d-state pairing

and spin-triplet (S = 1, p -or f-state) are formally possible.

The superconducting state is a many body state. The wavefunction for n electrons can be written as in analogy to the singlet-pair Cooper state

$$\Psi = \hat{P}\Psi(r_1, r_2), \Psi(r_3, r_4), \Psi(r_5, r_6)...\Psi(n-1, n) \tag{3.7}$$

where $\hat{P}$ is an antisymmetrization operator of interchange of any two electrons.

3.3 Ginzburg-Landau theory

Ginzburg-Landau theory is a phenomenological model to explain superconductivity. It doesn't give explanations for the microscopic phenomina, but examines the macroscopic properties of a superconductivity with the aid of thermodynamic arguments. The theory can be used to extend to both type I and type II superconductors. It has been proven that the GL theory is valid near T_c being in fact a limited form of the microscopic BCS-description.

The GL theory is based on Landau's general theory of second-order phase transitions. The Landau's theory was modified by Ginzburg and Landau for superconductivity and a complex pseudo-fuction as an order parameter was introduced. Near the superconducting transition the free energy F of a superconductor can be expressed in terms of a complex order parameter $\Psi(r)$. $|\Psi(r)|^2$ presents the local density of superconducting electrons $n_s(r)$. The theory was developed by applying variational method and working from an assumed series expansion of the free energy of Ψ and $\nabla\Psi$ with expansion coefficients alfa and beta, they derived differential equation for $\Psi(r)$,

$$\frac{1}{2m^*}(\frac{\hbar}{i}\nabla - \frac{e^*}{c}A)^2\Psi + \beta|\Psi|^2\Psi = \alpha(T)\Psi \tag{3.8}$$

The equation is nearly the same as the Schrödinger equation for free particle with an exception of a nonlinear term. The corresponding equation for the supercurrent is

$$J_s = \frac{e^*\hbar}{i2m^*}(\Psi^*\nabla\Psi - \Psi\nabla\Psi^*) - \frac{e^*2\hbar}{m^*c}|\Psi|^2\mathbf{A} \tag{3.9}$$

which is the usual quatum-mechanical expression for current of particles with mass m* and charge e*. With this kind of formalism the theory could take into account non-linear effect of the fields capable to change n_s and the spatial variation of n_s(or $\Psi(r)$).

The GL coherence length can be derived from GL differential equation. It turns out that $\xi(T) \approx \xi_0$ well below T_c, where ξ_0 is the microscopic BCS-coherence length. In the case where there are no fields present: $\mathbf{A} = 0$, the Ψ is real since there are only real cofficients. Thus we can write the GL differential equation in one dimension in a form

$$\frac{\hbar^2}{2m*|\alpha|}\frac{d^2f}{dx^2} + f - f^3 = 0 \tag{3.10}$$

where f is normalized wavefunction $f = \Psi/\Psi_\infty$. Thus it becomes reasonable to define the characteristic length for variation of $\Psi(T)$ as

$$\xi^2(T) = \frac{\hbar^2}{2m*|\alpha|} \tag{3.11}$$

The significance $\xi(T)$ as a characteristic length for variation of Ψ is evident when considering the GL differential equatiation in linearized form in which $f(x) = 1 + g(x), g(x) << 1$.

$$\xi^2(T)\frac{d^2}{dx^2} + f - f^3 = \xi^2(T)g(x)'' + (1 + g(x)) - (1 + 3g(x) + ...) = 0 \tag{3.12}$$

$$g(x)'' = (\frac{2}{\xi^2(T)})g(x) \tag{3.13}$$

$$g(x) \sim e^{\frac{\pm\sqrt{2}x}{\xi}} \tag{3.14}$$

which shows that a disturbance in Ψ decays on the characteristic lenght ξ. This is an important result when we discuss the superconductivity in 1-D in the next chapter.

The value of the characteristic length ξ can be calculated by eliminating coefficients α and β from the GL differential equations and setting $m^* = 2m_e$ and $e^* = 2e$:

$$\xi(T) = \frac{\Phi_0}{2\sqrt{2}H_c(T)\lambda_{eff}(T)} \tag{3.15}$$

where $\Phi_0 = \frac{hc}{2e}$ is the fluxoid quatum. The characteristic length is divided into so-called clean and dirty limits. The case when mean free path of an electron is larger than characteristic length is called the clean limit, and the opposite case is called the dirty limit. The BCS characteristic length is $\xi_0 = \hbar v_F/\pi\Delta(0)$.

$$\frac{\xi(T)}{\xi_0} = \frac{\pi}{2\sqrt{3}}\frac{H_c(0)}{H_c(T)}\frac{\lambda_L(0)}{\lambda_{eff}(T)} \tag{3.16}$$

when $T \approx T_c$

$$\xi(T) = 0.74\frac{\xi_0}{\sqrt{(1-t)}} \quad clean \tag{3.17}$$

$$\xi(T) = 0.855\frac{\sqrt{\xi_0 * l}}{\sqrt{(1-t)}} \quad dirty \tag{3.18}$$

The GL clean limit approximation is only valid in small range near T_c. The dirty limit approximation is valid in a broader temperature range.

3.4 Temperature dependece of the energy gap

The GL-model for the temperature dependece of the order parameter Δ is only valid near T_c. A more suitable model was needed to fit the experimental data. The temperature dependence for the energy gap and thus – also for the coherence length – was calculated using microscopic BCS model and numerical integration with suitable parameters attained from the experimental data.

$$\frac{1}{N(0)V} = \int_0^{\hbar\omega} \frac{\tanh(\frac{1}{2}\beta(\delta^2+\Delta^2)^{\frac{1}{2}})}{(\delta^2+\Delta^2)^{\frac{1}{2}}} d\delta \tag{3.19}$$

where $\beta = \frac{1}{k_b T}$. To simplify fitting procedure, once calculated using microscopic experession (3.19), the temperature dependence Δ(T) was approximated by simple analytical expression:

$$\Delta_{(T)} = 1.64(1 - T/T_c)^{1/2}(T/T_c)^{1.04/4}\Delta_0 \tag{3.20}$$

The equation is based on the GL approximation for the energy gap near T_c but has a term to compensate the saturarion of the energy gap at values $T << T_c$. The term itself doesn't have any physical meaning but works as a correction factor. The equation was fitted so that it is valid with high accuracy within the region $T > 1/4T_c$ which is the region of the fitted experimental data. A graph with different models for the temperature dependency is presented in Figure 3.5.

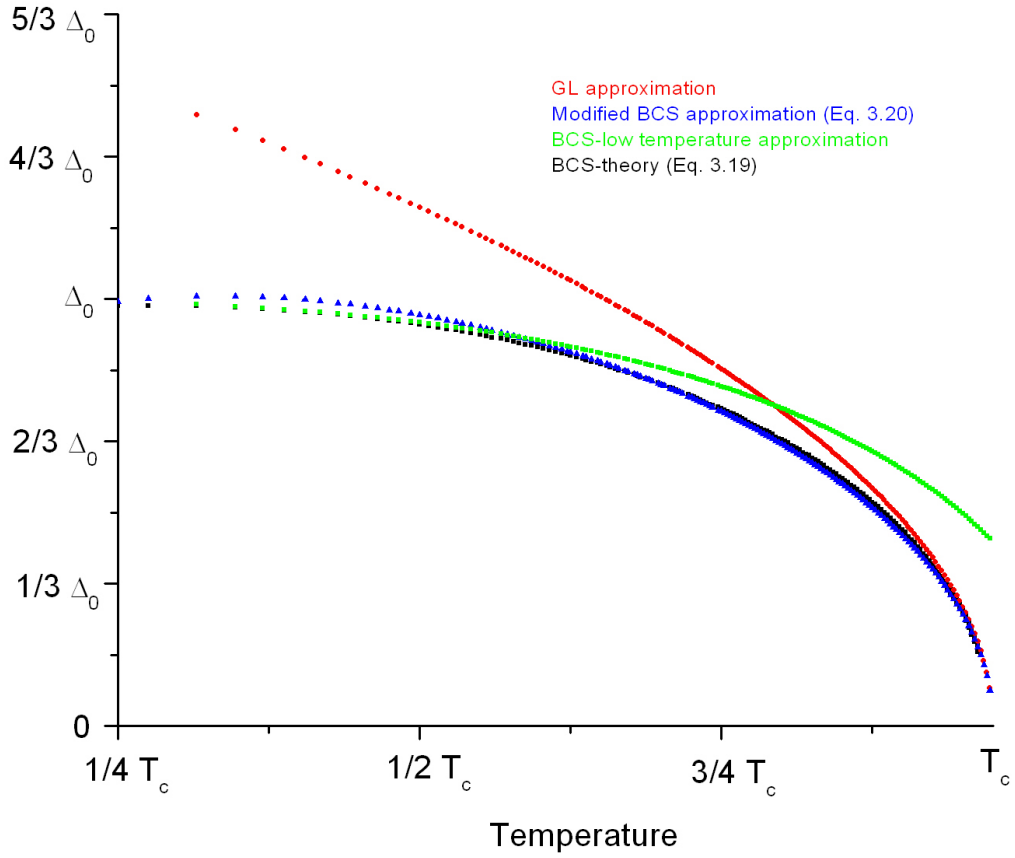

Figure 3.5: Different models for the temperature dependencies of the energy gap. The BCS-theory temperature dependency is calculated by numerical integration(Eq. 3.19). The modified BCS approximation in equation 3.20 is the one used for the data analysis.

3.5 Superconductivity in 1-dimension

3.5.1 General overview

In a homogenious 1D superconductor the sharp change in conductivity during phase transition, typical for 3D samples, is widened due to fluctuations of the superconducting order parameter which can lead to a non-zero resistance well below the critical temperature. One dimensionality requires that the dimensions of the wire are small compared to the superconducting coherence lenght and the magnetic penetration depth.

The qualitative explanation of the difference why the fluctuations play such a big role in 1D superconductors can be explain by means of Figure 3.6. At $T < T_c$ in 3D and 2D superconductors the fluctuations cause no changes: resistance R = 0. Regions with "normal" conductivity are shunted by the surrounding superconductor. As for the 1D-conductor, a fluctuation can block the supercurrent resulting in finite resistance.

The fluctuations in 1D superconductors can be divided to two classes by the mechanism causing the fluctuation. The first one is well known and experimentally well defined phenomena where the thermal fluctuations can supress the conductivity in the vinicity of the critical temperature. This leads to widening of the transition in the begining of the metal-superconductor transition. The other more disputed phenomina is the macroscopic quantum tunneling or quantum fluctuations of the order parameter. The effect is basicly the same as in the case of thermal fluctuations but as this process doesn't need external energy, being based on quantum tunneling, it may cause superconductivity to be suppressed even at T $->$ 0 K.

In Figure 3.7 is shown a qualitative picture of a the R(T) transition of an 1D-nanowire of dimensions in just above the QPS dominated regime. The thermal fluctuations play important role only in some millikelvin region in the vicinity of T_c. The effects QPS is shown in the lower part of the relatively sharp transition curve as it rounds significantly before reaching the zero resistance.

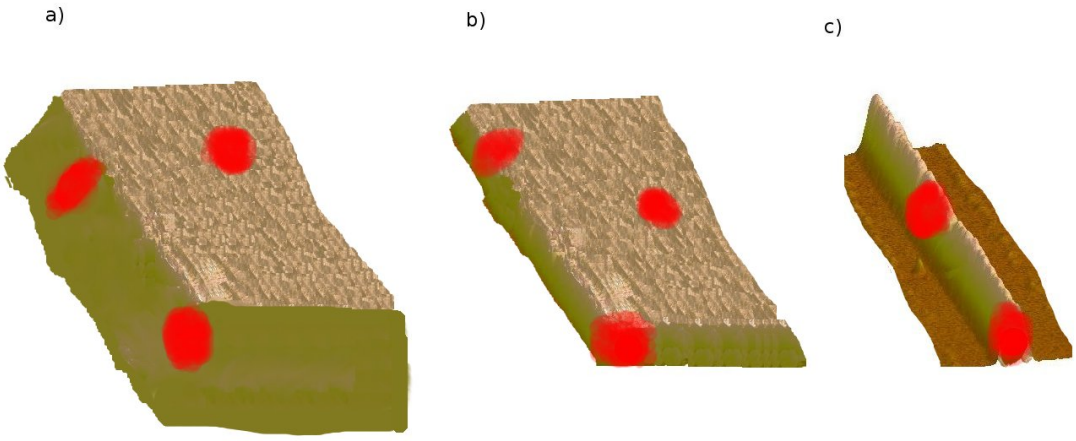

Figure 3.6: Qualitative picture of a) 3D superconductor b) 2D superconductor and c) 1D superconductor. The red dots are the fluctuation-induced regions with momentary suppressed superconductivity.

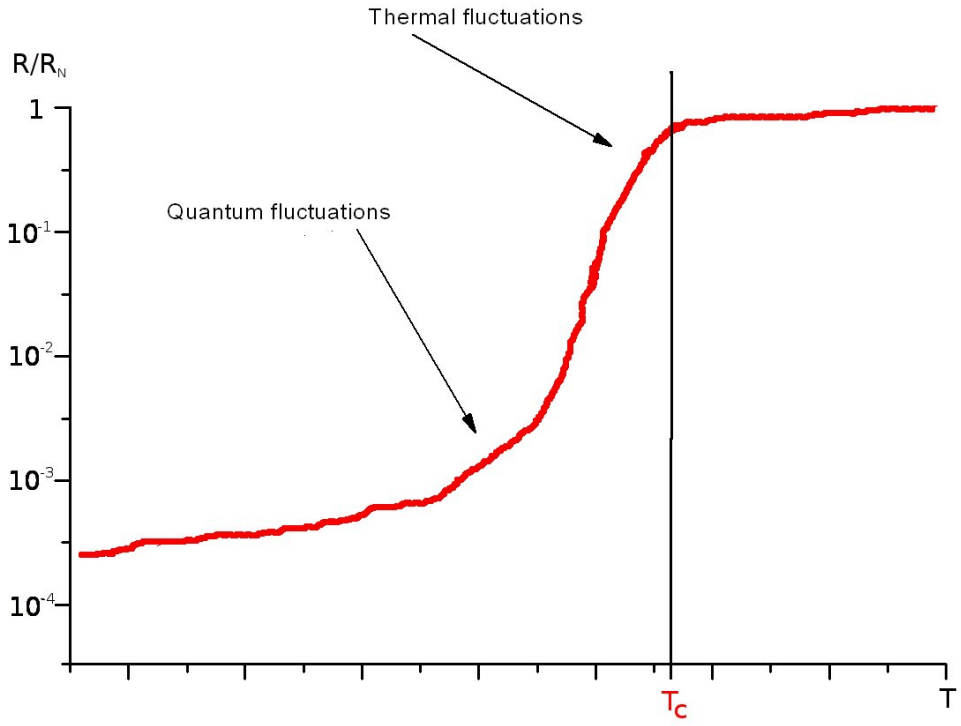

Figure 3.7: A typical looking transition curve of a sufficiently narrow nanowire.

3.5.2 Concept of a phase slip

The idea of phase slips was first introduced by W. Little[2]. He consider that thermodynamic fluctuations in very thin wires could be detectable. He also showed that a true phase transition of an infinitely sharp change in resistivity is possible only in an specimen with three infite dimensions. The basis of the calculations was within the GL model by minimizing the free energy expressed by the GL functional in one dimension.

$$F(\Phi) = \int [a|\Phi(x)|^2 + b|\Phi(x)|^4 + c|\Delta\Phi(x)|^2]dx. \tag{3.21}$$

The order parameter $\Phi(x)$ is a complex function with real amplitude $\Delta(x)$ and phase $e^{i\phi(x)}$. In the usual case the fluctuations are ignored and the equilibrium value for $\Phi(x)$ is calculated by minizing $\Delta(x)$ and $\phi(x)$. Other functional form of $\Delta(x)$ and $\phi(x)$ are still possible with a probability propotional to the Boltzman factor $e^{-\beta F(x)}$. Basicly this means that in the vicinity of transition temperature there is a probability that the temperature fluctuations may allow the order parameter to diffuse to higher free-energy states.

The requirement for persistent current in a ring-shaped superconductor is that the line integral of the order parameter around the ring is multiple of 2π. The supercurrent is due to the gradient of the phase and the phase can only change an integer times 2π. A metastable supercurrent thus corresponds to the phenomenon of fluxoid quantization associated with integer winding number. When a supercurrent decays, it can only decay by discrete amount due to the change of the winding number. When the results are translated into a singly connected superconducting wire, the conclusions is that the ends of the wire retain a constant relative phase ϕ_{12} while the perfect conductivity requires that the potential difference between the ends of the wire is zero. This means that the supercurrent will fluctuate to keep the total current constant(kept by external source) resulting in finite voltage across the sample. These fluctuations won't be averaged-out in limited time spawn perfectly, but a finite voltage is left $\overline{V}$.

If a superconducting nanowire has a finite resistance the averaged phase differ-

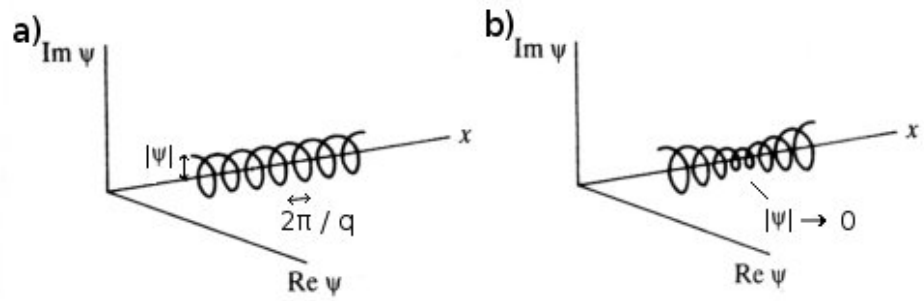

Figure 3.8: After M. Tinkham.[3] a) Uniform solution of complex current-carrying GL equation in one dimensional superconductor presented as Aragand diagram. b) Non-uniform solution where the helix is tightened and $|\Psi| -> 0$ i.e. just before phase-slip happens.

ence ϕ_{12} should increase steadily with time. The solution for this apparent inconsistency is that phase-slip events occur, in which the phase coherence is momentarily broken, at some point(s) of the superconductor. To maintain this steady state condition and following the Josephson relation such events much occur with frequency

$$\frac{2eV}{h}, \tag{3.22}$$

where the $\overline{V}$ is time-averaged voltage. This means that the relative phase difference increases in time untill a phase slip process occurs reducing the phase difference ϕ_{12}.

The steady superconducting current in equilibrium is visualized in the Figure 3.8a. The complex parameter is expressed in polar coordinates. The solution for $J < J_c$ is can be presented by helices of pitch $\frac{2\pi}{q}$ and radius Ψ_0. The presented equilibrium solution is of the flow for current at zero voltage.

If a voltage is applied the relative phase difference between wire ends increses at steady rate as was earlier discussed

$$\frac{d\phi_{12}}{dt} = \frac{2eV}{\hbar}, \tag{3.23}$$

This can be visualized by the phase being cranked and kept steady at one end(Figure 3.8b). This simply describes the acceleration of the supercurrent explained by the London equation.

$$\frac{\partial \mathbf{j_s}}{\partial t} = \frac{n_s e^2}{m} E, \tag{3.24}$$

which means that the presence of voltage increases q untill the phase difference between the ends of wire obey $\phi_{12} = qL$ or from the London equation

$$\frac{\partial \mathbf{v_s}}{\partial t} = \frac{e\mathbf{E}}{\mathbf{m}} \qquad (j_s = n_s e v_s) \tag{3.25}$$

When the v reaches the limit of v_c the uniform solution is no longer possible. The phase slip processes maintain the steady state with $v_s < v_c$, in the presence of non-zero voltage, if the turns of the helix are annihilated by the rate of the new ones are being crancked. This means that energy is transferred at a rate of IV which is dissipated as heat or phonon emission rather than being converted to the kinetic energy of the supercurrent.

Langer and Ambegaokar presented a theory that is based on the Ginzburg-Landau equation constructed in analogy with the droplet model of a supersaturated vapor[4]. Just as in the droplet model the fluctuations are extremedly improbable and play no role determing the bulk properties of system. The model equates the constantly increased current caused by non-zero voltage with fluctuations reducing the phase difference.

Neglecting the normal currents the conservation of the current requires that supercurrent is constant. The current is the change of the phase and the density of superconducting electrons is expressed through the order parameter we'll get

$$|\Psi|^2 \frac{d\phi}{dx} = I = constant \tag{3.26}$$

which serves as constrait on variations of order parameter. If the order parameter is small on some point, the $d\phi/dx$ must be large. Thus when $|\Psi| - > 0$, it is easy to substract or add a turn[2]. What Langer and Ambegaokar did was to use this idea and find a path through function space where two uniform solutions with different amount of turns have the lowest free-energy barrier to overcome. This way they found the saddle point barrier of the GL free energy. By this they calculated the saddle-point free-energy increment,

$$\Delta F_0 = \frac{\sqrt{2}H_c(T)^2}{3\pi} A\xi, \tag{3.27}$$

where A is the area of the conductor and ξ is the characteristic length of the GL theory(3.15) and H_c is the temperature-dependant critical magnetic field. It can be thus deducted that the free-energy barrier is reduced when the wires cross section is is reduced. The energy is also about the same as condensation energy of a length of wire of $\sim \xi$ which is plausible since one can argue that the Ψ cannot vary more rapidly than the coherence length.

In the absence of voltage bias, the phase slips $\pm 2\pi$ are equally as probable. When a finite voltage is applied the slips in one direction become more probable than in the other. The energy of jump is different to different directions in the phase space. This difference stems from the electrical work done in the process. The model can be derived by modeling the slip as resistively and capacitivily shunted junction[3]. For a phase slip of 2π the energy difference is

$$\delta F = \Delta F_+ - \Delta F_- = \frac{h}{2e} I \tag{3.28}$$

McCumber showed that Langer and Ambegaokar arguments can be used as well when constant current instead of constant voltage[5]. This is the typical case when superconducting nanowires are measured experimentally.

The phase slip rate can be calculated if we'll take an unkown prefactor Ω. The prefactor is so called attempt frequency. The attempt frequency is dependent on the wires length since we could expect that the slips should happen independantly from each other.

$$\frac{d\phi_{12}}{dt} = \Omega[e^{\frac{-\Delta F_0 - \frac{\delta F}{2}}{k_B T}} - e^{\frac{-\Delta F_0 + \frac{\delta F}{2}}{k_B T}}] = \frac{2eV}{\hbar} \tag{3.29}$$

The correlation between voltage and current in wire undergoing phase slips can be resolved from the equation 3.29 using the result 3.28. In Figure 3.9 the phase slip process in situation where there is finite electric current is described by the tilted washboard model.

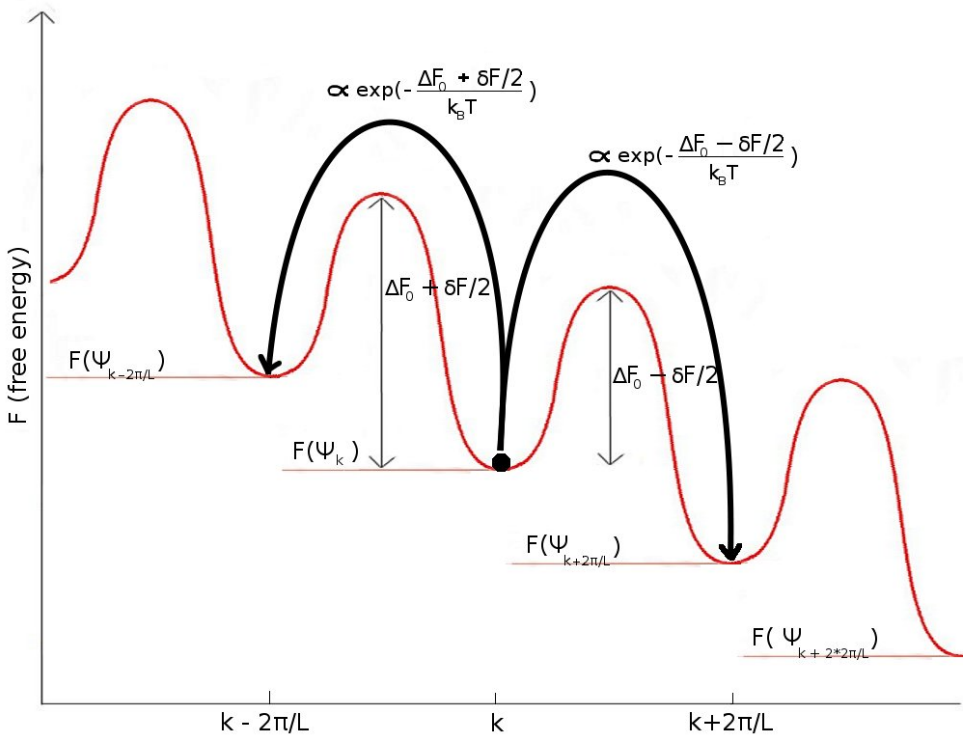

Figure 3.9: The washboard model with finite current describing the thermal phase-slips energy scale and rate to different directions.

McCumber and Halperin derived equation for the attempt frequency using time dependant GL-theory(TDGL)[6].

$$\Omega = \frac{L}{\xi}(\frac{\Delta F_0}{kT})^{\frac{1}{2}}\frac{1}{\tau_s} \tag{3.30}$$

where τ_s is the characteristic relaxation rate of the supercurrent in the TDGL. Thus an attempt frequency is resolved and using equations 3.29 and 3.28 for voltage current correlation

$$V = \frac{\hbar\Omega}{e}e^{\frac{-\Delta F_0}{k_B T}}\sinh(\frac{hI}{4ekT}) \tag{3.31}$$

a model for the normal metal - superconductor transition is derived. The model is called LAHM(Langer-Ambegaokar-McCumber-Halperin).

For the experimental fitting the resistance caused by the TAPS needs to be calculated. For simplicity we can assume small currents approximation which replaces the hyberbolic sine by its argument and by using the Ohm's law the resistance can be calculated.

$$R_{TAPS} = \frac{V}{I} = \frac{\Omega\pi\hbar^2}{2e^2k_BT}\exp(\frac{-\Delta F_0}{k_BT}) \tag{3.32}$$

The approximation is valid when $I < I_0$, where

$$I_0 = \frac{4ek_BT}{h} = 0.0013\frac{\mu A}{K} \tag{3.33}$$

at lowest temperature reachable with the cryostat used in the experiment $\sim 50mK$ the maximum current is

$$I_0 * 0.050K \approx 0.67nA \tag{3.34}$$

which is smaller than the AC-currents used in the R(T) measurements, which where roughly 50 pA - 200 pA.

The LAHM model and the theory is verified by several experiments. The most well known experiements are the measurements of resistive transition and the current-voltage characteristics of single-crystal tin whiskers[7, 8]. The thermally

activated phase slips proposed by Langer and Ambegaokar were observed and their contribution, determined by the rate of phase slippage, was verified with the modification of the attempt frequency proposed by McCumber and Halperin.

The weak point of the model is that it only works at values just below the transition temperature. The LAHM theory doesn't work when temperature approches T_c since the attempt frequency and free-energy barrier go to zero at T_c. In the other hand the model is based on GL theory which works only values $T/T_c \approx 1$.

3.5.3 Microscopic model of Quantum Phase Slips

When temperature drops the number of thermally activivated phase slips is reduced exponentially and no resistance should be expected when T is much smaller T_c based on the earlier calculations. Recent experimental results have shown the opposite and many theoretical models to explain the phenomina have been made. The explanation is that instead of thermally activated phase slips, phase slips by quantum tunneling start to be of the essence.

The first models gave phase slip rates that couldn't explain the experimental work. A first estimate for the QPS tunneling rate $\sim e^{-S_{QPS}}$ leads to a disappointing conclusion, because of exaggerated QPS action term, which roughly equals the number of transverse channels $S_{QPS} \sim N_{ch} = {k_F}^2 A$ in a wire of cross section A[9]. This gives a huge value for even really thin nanowires. When the diameter is about ~ 10 nm the S_{QPS} would be about $10^2 - 10^3$ and therefore the QPS should be highly suppressed. Further it has been argued that the rate should be reduced by the fine structure constant $\alpha = 1/137$. This is because the supercurrent in one dimension is not a charge neutral process but involves an electromagnetic field which affects the decay rate[10].

Golubev and Zaikin(GZ) argued that the estimation needs qualitative improvement[11]. The first approximation they made was to take into consideration the finite dimension $l < 10$ nm of the measured nanowires. The coherence length $\xi \sim \sqrt{l\xi_0} << \xi_0$ should be taken as the typical QPS size. They also argued that the role of electromagnetic field should be smaller than that was calculated

earlier. Third thing was to presume that dissipative currents should not have strong impact on the QPS rate when T is significantly smaller than T_C. They also switched the calculations from the TDGL-model used earlier to microscopic level making a microscopic QPS model.

The GZ model has the QPS rate in a following form

$$\tau_{QPS} = \Omega e^{-S_{QPS}} = \Omega e^{-(S_{out}+S_{core})} \tag{3.35}$$

The action S_{QPS} is divided into two term; the term S_{core} considers the phase slip center and it is determined by the condensation energy and dissipation of the normal currents. The S_{out} a hydrodynamic part which is dependent of the propagation of electromagnetic fields out of the phase slip center. The evaluation of S_{out} is much simplified by the fact that outside the core the absolute value of the order parameter remains equal to some mean value and only the phase of the order parameter changes. The S_{out} saddlepoint action is in the form

$$S_{out} = \mu \ln [\frac{\min (c_0\beta, X)}{\max (c_0\tau_0 x_0)}] \tag{3.36}$$

where $c_0 = \frac{1}{L_s C_l}$ is the Mooij-Schön plasmon velocity [14], C_l is the wire's capacitance per unit length, the x_0 and τ_0 are the typical length and time scales of the QPS event.

$$\mu = \frac{\pi}{4\alpha}\sqrt{\frac{C_l}{L_s}} \tag{3.37}$$

is a dimensionless parameter describing the characteristics dampening of the electromagnetic excitations, where α is the fine structure constant, C_l and L_s the capacitance and inductance per unit lenght. For infinitely long wire, the S_{out} at the limit of $T- > 0$ diverges logarithmically towards zero making the QPS action of the term highly improbable.

The another part of the S_{QPS} is the core contribution. The calculation of the core action parameter is a formidable task but if a dimensionless prefactor which is fitted from the experiments is added the calculations are much simplified. This allows to approximate the order parameter field inside the QPS core by two types of

fluctuations. The absolute value of the the order parameter should vanish at limits $x = 0$ and $\tau = 0$ and coincide the mean field value outside the QPS core. The phase should flip at $x = 0$ and $\tau = 0$ providing change of the net phase 2π. This leads to a trial function describing the dynamics of the phase slip[12].

$$|\delta\Psi(x,\tau)| = \Psi_0 exp(-\frac{x^2}{2{x_0}^2} - \frac{\tau^2}{2{\tau_0}^2}) \tag{3.38}$$

Minimazing the action S_{core} with respect to x_0 and τ_0 it is possible to get result for the core parameters and the core action.

$$x_0 = a\sqrt{\frac{D}{\Psi_0}} \approx \xi \tag{3.39}$$

$$\tau_0 = \frac{b}{\Psi_0} \approx \frac{\Delta_0}{h} \tag{3.40}$$

$$S_{core} = \pi A N_0 \sigma \sqrt{D\Psi_0} = A\frac{R_q L}{R_N \xi}, \tag{3.41}$$

where a, b, A are the dimensionless prefactors, R_N is the total normal state resistance, $R_q = \frac{\pi\hbar}{2e^2} = 6.453\ k\Omega$ is the quantum resistance. The QPS rate can be approximated $S_{QPS} \approx S_{core}$ for sufficiently short nanowire in which the capacitive effects are small enough because then $S_{core} >> S_{out}$. The limit where the approximation works best is

$$L << \xi\frac{e^2 N_0 \sigma}{C_l}. \tag{3.42}$$

This limit is around 10 μm depending on the wire's material. In the longer wires the capacitative effects also affect the core part and the separation of the action terms isn't an ideal approximation. In the experiment, the used wires are about two times longer than the limit, but still well within the limit where the approximation works well enough compared to the experiment's accuracy. On the opposite limit for sufficiently long nanowires $l > 100\ \mu m$ the core action takes a bit more complicated form

$$S_{core} = \frac{CR_q}{R_N}(\frac{X}{\xi})^{\frac{3}{2}}\sqrt{\frac{C}{e^2 N_0 s}}, \tag{3.43}$$

where C is a numerical prefactor.

These models give for S_{QPS} action about ~ 2 orders of magnitude smaller term than the first estimates of QPS actions and gives results that QPS should be observable for sufficiently thin wires even at $T \approx 0$.

The prefactor Ω can be calculated by instanton techinique giving it a form

$$\Omega = \frac{BS_{QPS}L}{\tau_0 x_0} \tag{3.44}$$

where B is a numerical constant of order of unity. Thus QPS rate for nanowires can be written using equations 3.35, 3.37, 3.42 and 3.44.

3.5.4 Resistance of the nanowire below T_c

The QPS rate for the nanowires in the zero current limit is set by the equation 3.35. A fairly heuristic model for calculating the resistance cause by QPS with small currents can be made by using similar expressions as in the LAHM model's derivation for non-zero small currents and proceed the same way as in the derivation for resistance caused by TAPS. This gives a formula, which is relatively close to ones given by more advanced calculations, but the derivation is more easily understandable[13]. Let's write the action in form

$$S_{QPS} = \frac{\Delta F_0}{E_{ch}}, \tag{3.45}$$

where E_{ch} is characteristic energy scale of the QPS process. It's value is given by the Heisenberg uncertainty principle and the in the GZ derivation it corresponds to the superconducting gap $\Delta_0 = \frac{h}{\tau_0}$. Using this result the phase slip rate calculated as of non-zero current

$$\tau_{QPS} = \tau_- - \tau_+ = \Omega \exp(\Delta F_0 - \delta F/2) - \Omega \exp(\Delta F_0 + \delta F/2)$$

$$= 2\Omega \sinh\left(\frac{\delta F}{2E_{ch}}\right) \exp\left(\frac{-\Delta F_0}{E_c h}\right). \tag{3.46}$$

The voltage and the resistance can be derived in the analogy of the LAHM model 3.31.

$$V_{QPS} = \frac{h}{2e\tau_{QPS}} = \Omega \frac{h}{e} \sinh\left(\frac{hI}{4eE_{ch}}\right) \exp\left(\frac{-\Delta F_0}{E_{ch}}\right) \tag{3.47}$$

$$R_{QPS} = \frac{V_{QPS}}{I} = \frac{\Omega R_q h}{E_{ch}} \exp\left(-S_{QPS}\right) \tag{3.48}$$

The E_{ch} doesn't affect the exponent term and as such the action can be substituted back to it. E_{ch} appears only in the prefactor Ω. This gives formalism which works well within temperature region valid for GL-model.

$$R_{QPS} = B\frac{L}{\xi(0)} R_Q (1 - T/T_c) \exp\left(-S_{QPS}(T=0)(1-T/T_c)^{1/2}\right) \tag{3.49}$$

The model used for theoretical fittings used for fitting the experimental data is a little more complicated to derive as it is based on the microscopic model of superconductivity. The heuristic model calculated above still gives result identical results but has an disadvantage having physical parameters included within the fitting parameters. The experission used for the fitting the data is

$$R_{QPS} = b{S_{QPS}}^2 \Delta(T) \frac{L}{\xi(T)} \exp\left(-2S_{QPS}\right) \tag{3.50}$$

where b is a fitting parameter[12]. The most simple model for QPS fits only takes into account the core action which is a valid approximation for sufficiently short wires. Also the fitting parameter isn't a dimensionless in the equation and as such has physical meaning. There are several possibilities for the parameter. The parameter most likely has a form of $b = \frac{R_N}{\Delta_0}$. Using equation 3.42 for the core action the equation can be written in form

$$R_{QPS} = R_N \left(A\frac{R_q L}{R_N \xi(T)}\right)^2 \frac{\Delta(T)}{\Delta_0} \frac{L}{\xi(T)} \exp\left(-2A\frac{R_q L}{R_N \xi(T)}\right) \tag{3.51}$$

The parameter A is a dimensionless parameter of order of unity describing the magnitude of the QPS action and it is used as a fitting parameter when making the theoretical model.

3.6 Quantum mechanical standard for current - phase slip junction

Theoretical predictions give a rise to an idea to treat the phase slips centers as Josephson junctions. The behavior of such QPS junction should be exact dual of the Josephson junction which can be used as voltage standard when current biased. The properties of phase-slip junctions are identical to those of Josephson junction when the voltage is exchanged to current. For example Josephson junction biased with small current is perfect conductor as phase-slip junction biased with small voltage is perfect insulator.

Under microwave irradiation current biased Josephson junction has flat voltage plateaux and as such it can be used as voltage standard. The same method should be applicable with phase-slip junctions. In Figure 3.10 a qualitative presentation of the IV characteristics of an imaginary nanowire within the limit of quantum fluctuations under microwave radiation.

There are several conditions for a structure that could be used as current standard. Superconductor dimensions should be well within the limits of quantum fluctuations which based on the experiments results is for titanium around 30 nm. The wire must have high resistance to provide damping $R > R_Q = h/4e^2$ and the resistance must be maintained under microwave irradiation. The transition temperature of the wire needs to be high enough that the nanowire can be refridgerated well below the T_c to be sure to observe only quantum fluctuations.

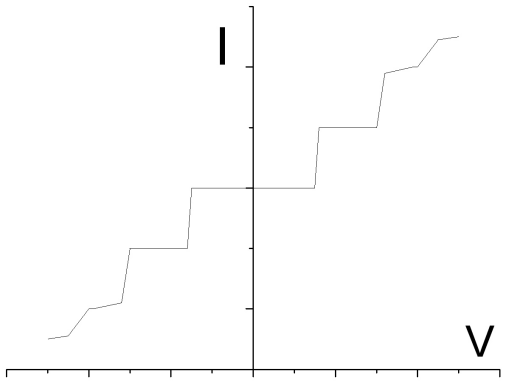

Figure 3.10: Qualitative picture of IV-characteristics of an imaginary superconducting nanowire within limits of quantum fluctuations under microwave irradiation.

3.7 Resistance of a nanowire in normal state

The normal state conductivity of a nanowire has several factors that needs to be considered in order to get a reasonable model. Using only the free electron model may give values of decades wrong. The main additional factors that need to be taken into account are additional scattering from the surface as well as grain boundaries of the conductor. Also the valence of the wire may vary from the bulk value. Many models have been developed. The most sophisticated ones have give quite good predictions of the size dependency of the resistance.

For the experiments point of view it is enough to know that the resistance of the nanowire has additional factors which will highly increase the resistance in the limit of sub-50 nm wires. The resistance of narrow nanowire can't be linearily scaled down and the structural differences between wires in this scale can cause very large differences in the resistance even if the cross-sectional area of the wire would be the same.

3.8 Sputtering

The physical sputtering working mechanism is momentum exchange between the incident ions and the atoms of the target material due to collisions. Sputtering is normally done by forming a gaseous plasma and then accelerating the ions from this plasma into some material. When the ions hit the target there is a cascade of collisions. If the energy of the atoms reaching the surface is high enough compared to the binding energy of the surface material, atoms of the target can be ejected.

3.8.1 Qualification of different sputtering regimes by the ion energy

The sputtering can happen in three qualitatively different ways; in the single-knockon regime, the linear cascade regime and the spike regime. In the single-knockon regime the bombarding ion transfers it's energy to the target atoms which, if energetic enough, are ejected through the surface (Figure 3.11a). The regime falls into lower and medium eV energy region except for very light ions. In the linear cascade regime the incident ions cause atoms to recoil and thus atoms hitting other atoms in the target material can also be ejected (Figure 3.11b). The characteristic energy of the ions for this regime are in the order of keV and MeV depending on molecular masses. The spike regime differs from the linear cascade region by the spatial density of moving atoms(Figure 3.11c). The energies are in the same range as in the linear cascade regime, but the ion masses are normally a significantly larger.

3.8.2 Estimation for the sputtering rate

The ion beam etching in the experiment was done with 1 keV argon ions. The penetration depth into titanium can be easily calculated by Monte Carlo simulation of the process. A simulation done using SRIM program gives values for the penetration depth about 1 - 2 nm. The sputtering is happening well within the single-knockon regime and it has been proven to be non-destructive when used in small dosages at a time[15].

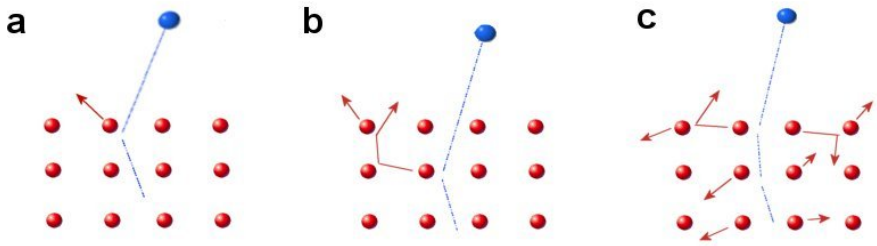

Figure 3.11: The regimes of sputtering a) the single-knockon regime b) the linear cascade regime c) the heat spike regime.

By combining mean-free-path and penetration depth and adding a correction term as not all the collisions eject an atom even if the energy is high enough. The sputtering yield can be calculated.

The incident angle of the beam changes the penetration depth. The beam approximately travels the same distance but the beam coming from an angle travels it closer to the surface.

The sputtering rate can be estimated by intensity of the ion beam hitting the target, the sputtering yield and the redeposition rate. The sputtering yield only gives the amount of ejected atoms per incident ion so a term is needed to approximate yield into average volume of material ejected per incident ion. A simple equation for sputtering rate can be now formulated combining these factors.

$$S_R = \frac{IY(E_P)M}{\rho N_A} \tag{3.52}$$

where I is the ion current per square centimeter, Y is the sputtering yield, ρ is the density of the target material, M is the molar mass of the target and N_A is the Avogadro number.

The sputtering yield for the calculations is normally taken from simulations. Usually it is more important to know the depth of sputtering crater which can be calculated by integrating the current over time.

$$d = \int_0^t \frac{IdtY(E_P)M}{\rho N_A} \tag{3.53}$$

The equation gives a theoretical value for sputtering crater depth. In reality some of the material is redeposited and some part of the measured current is due to electron cascades generated by the collisions with the incident beam and the target. Taking these into to account the we get an equation

$$d = \delta_I \delta_{R(p)} \int_0^t \frac{IdtY(E_P)M}{\rho N_A} \tag{3.54}$$

where δ_I is the error in the current measurement, $\delta_{R(p)}$ is the redeposition rate function with the pressure as a variable.

3.8.3 Evolution of the wire cross-section with sputter-etching

The sputtering crater depth is dependant of the simulated yield which may be different than the realistic yield. Thus the final value for the reduction of the cross section can be more accurately calculated if the total fluence for sputtering the whole structure is known. In practice this is done by etching the remaining metal and by comparing AFM measurements before and after the etching. This is the case when the structure is totally sputtered and the remaining cross section is measured. The shape of the cross section is approximated with a trapezoid which is a typical for lift-off fabricated nanowire. The are of the trapezoid is decreased with sputtering like a parabola[13]. The result for a evolution of the cross section which preserves its shape during sputtering is,

$$\sigma = \sigma_0 (1 - \frac{\phi}{\phi_0})^2, \tag{3.55}$$

where σ_0 is the initial cross section, the ϕ_0 fluence needed to sputter away the whole structure and ϕ is the fluence so far.

Chapter 4

Sample and the measurement setup

4.1 Sample's layout

The measurements were made with two different types of titanium nanowires. The first ones were made to measure the properties of the titanium nanowires within the regime of quantum fluctuations. These samples consisted only superconducting titanium elements in order to get the wire measured the best possible accuracy. The other structure had a titanium nanowire constructed within high resistive environment. This environment was made by using dirty titanium which had the superconductivity suppressed well below 70 mK.

A SEM image of the nanowire fabricated for the QPS studies is presented in Figure 4.1. The wire's lenght is about 30 μm and dimension at the begining 60 nm x 57 nm. The distance between the voltage probes is 19.7 μm. The wire's cross section was later on reduced by sputtering. This requires that the wire doesn't have any constrictions as such places would be sputtered faster than the rest of the wire. For that reason the wire's cross section at first is higher than the expected limit for QPS as more uniform wire is easier to make that way.

The mask for the nanowires was made using e-beam lithography with single layer resist. After the patterning and the development of the mask the structure

was cleaned with reactive ion etching using low energetic oxygen plasma. This step was made to be sure that no resist would be left on the surface of the silicon that could break the narrow wires during cool down or contaminate the evaporated material. The metal evaporations were done in UHV electron beam evaporator with zero angle evaporation. The evaporation of titanium can be challenging as it needs good vacuum and clean chamber to have low impurity level and thus reasonably high Tc.

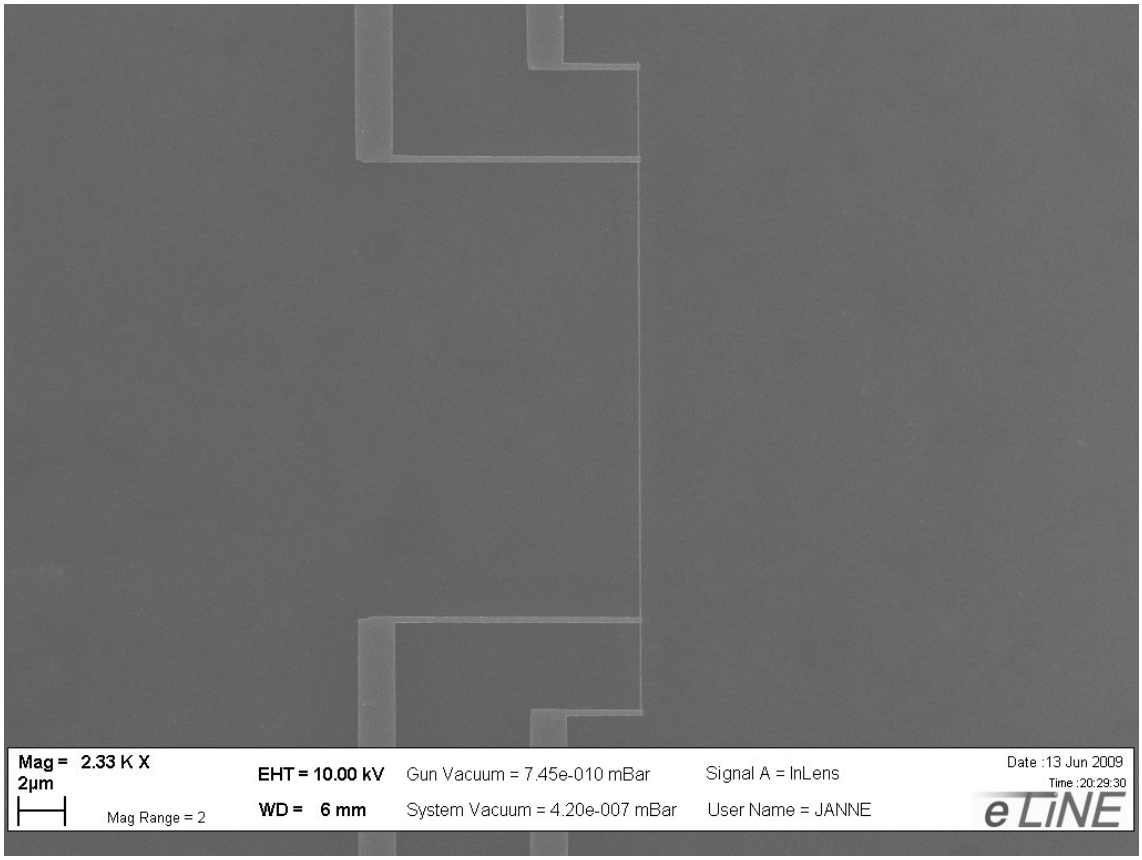

Figure 4.1: A SEM image of the nanostructure used in the QPS studies containing the titanium nanowire with dimensions of 60 nm x 57 nm and four probes attached to it for four-probe electrical measurements.

The second sample consisted of two types of titanium wires; one narrow with reasonably high superconducting transition temperature and four highly resistive titanium resistor wires that had the superconductivity suppressed. The structure was done with e-beam lithography using double layer resist. The double layer resist

somewhat lowers the best possible accuracy of the patterning but it is necessary because the structure was to be made with angular evaporation. In earlier structures it was found that if titanium was evaporated at high angles it didn't have the superconducting transition. Thus it gave an idea to use titanium as resistor and superconductor in the same structure. This gives an advantage when the wire needs to be sputtered in order to reduce dimension as the contanimination from the nearby materials could be a problem and it also ensures that the sputtering rate is the same for the nanowire and for the resistors. Also the resistor lines heat up during the measurement and there could be a small temperature difference between the superconducting wire ends which could cause Seebeck voltage to affect the measurement if the materials were different, though the effect should be negligible at these ultra low temperatures. SEM picture of the sample is presented in Figure 4.2.

There are several possible reasons why the at high angles evaporated titanium didn't go into superconducting state. The first idea was that the evaporation rate is so much smaller that the titanium contaminates on the way to the sample as the effective evaporation rate is reduced by the cosine of the evaporation angle due to the change in area respect to the evaporation crusible. The effect was compensated by increasing the rate. This didn't seem to affect the result at all. Next idea was that the undercut area where the angularily evaporated titanium is mainly deposited is more dirty since the RIE oxygen flash doesn't clean the undercut areas as well as the open areas. This possibility was tested and found quite unlikely since even though a wire is evaporated from an angle that is in line with angle of the evaporation, which should correspond in this sense the situation of zero angle evaporation, the wire doesn't have superconducting transition. One likely possibility is is that the angularily evaporated titanium is contaminated by the edges of the resist. If this is the case then the effect most likely should be seen also in very narrow titanium wires. The smallest lines manufactored to had dimension about 50 nm x 45 nm but still had a superconducting transition.

It can be observed that the surface of the angularily evaporated titanium has grains growing in step-like pattern within the line evaporation angle (Figure 4.3).

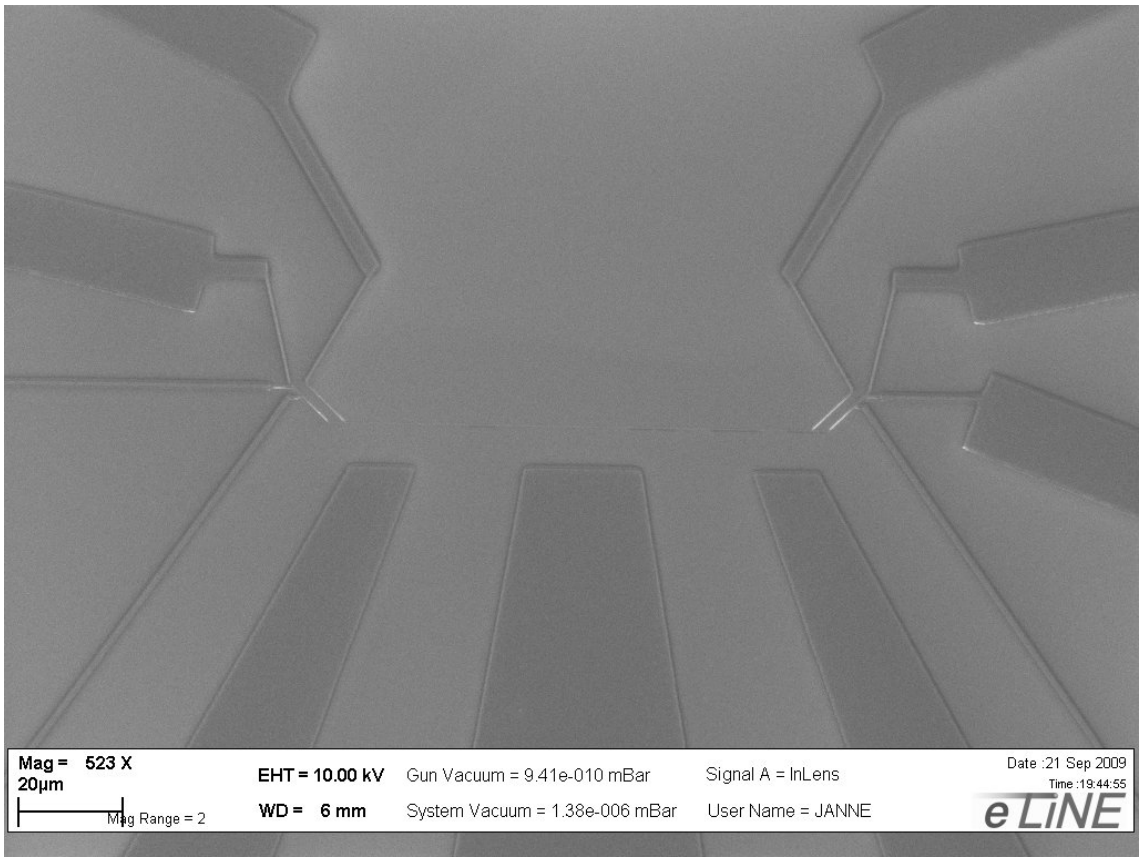

Figure 4.2: A SEM image of a nanowire in highly resistive environment. The four highly resistive probes connected to the titanium wire are made out of titanium using angular evaporation. The titanium nanowire is made with zero angle evaporation and has dimensions 50 nm x 45 nm.

Based on observations of the images it is possible to say that there could be some plane defects which may result in an unexpected behaviour.

The sample also have an antenna which can be used to expose the nanowire with high frequence RF signal. This feature is for later experiments which aim at making quantum standard for electric current. Also one big difference is the lenght of the nanowire. The first nanowires fabricated were already relatively long around 30 μm but for the second structure the length of the nanowire was still to be increased to get the proximity effect caused by the normal metal resistors small enough compared to the normal state resistance of the nanowire and that the antenna could fit next to the wire. The nanowire length is roughly 90 μm and the distance between the

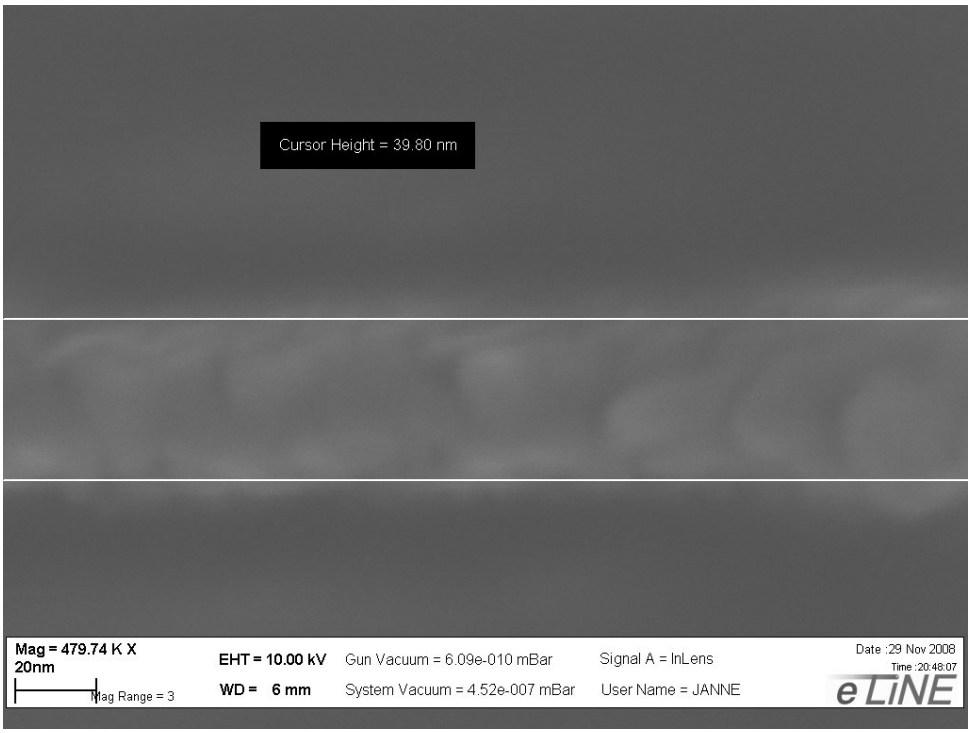

Figure 4.3: A SEM image of the angularily evaporated titanium nanowire. The titanium was evaporated at angle of 45 degrees from the "right" side and within the line of the mask.

voltage probes about 85 μm.

4.2 Measurement setup

All the samples were measured in same type of configuration. The circuit is presented in Figure 4.4. When the DC-bias wasn't needed the DC-voltage source was detached and the connection grounded.

The low temperature measurements were made with a dilution refigerator. This technique has been in use for several decades and has been widely used for research purposes. Dilution refrigeration with optimized ^{3}He/^{4}He mixture makes possible to reach few millikelvin stable temperatures. Normally temperatures in modern refrigerators are in order of some tens of millikelvins as was in ours which is capable to reach about 60 mK temperature[16].

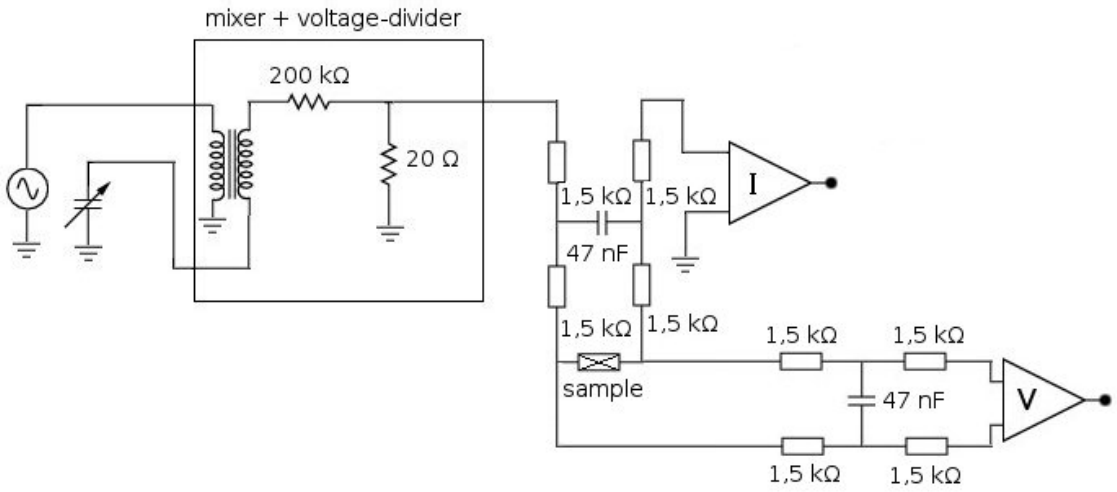

Figure 4.4: Circuit diagram of the four-probe measurement setup used in the experiments.

Chapter 5

Results

5.1 Experimental study of quantum fluctuations in titanium nanowire

5.1.1 Fabrication and properties of the titanium nanowire

The sample for the study was made to be as simple as possible. The whole structure was made out of high purity titanium giving it comparably high transition temperature. As was already discussed the evaporation in UHV conditions doesn't guarantee the good quality of the titanium but also many other factors need to be considered.

The sample was sputtered several times with small ion fluxes and re-measured after each sputtering. The study of the evolution of the wire can be done continously with the same wire and as such the results are not affected by the differences in the manufactoring processes. The sample contains only titanium and silicon substrate making the possible contaminations during the sputtering rather unlikely. The sputtering polishes the sample but large features tend to grow in contrast as the sputtering progresses. In Figure 5.1 is a comparison of the nanowire before and after the sputtering.

The first measurements were done with two nanowires with dimensions 60 nm x 57 mn. The distances between the voltage probes were about 19.7 μm. The

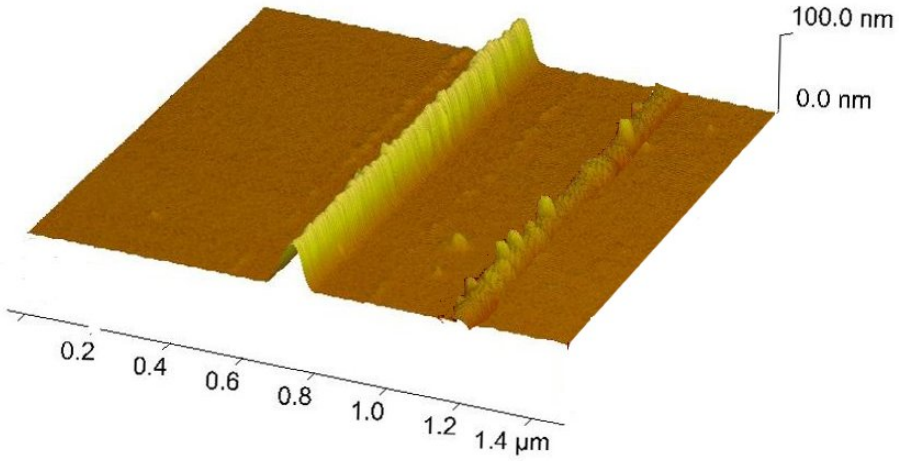

Figure 5.1: AFM image of a nanowire before and after the sputtering. The horizontal resolution of the images is limited by the AFM tip radius and thus the horizontal width doesn't change in the images.

resistances of the wires were 19346 $\pm$ 4Ω and 19763 $\pm$ 5Ω at 1 K. The resistivity calculated as an average value between the two values is about 334 $\mu\Omega\ cm$. The normal state mean free path calculated using Drude-model and table value for fermi energy 8.15 eV is about 2 Å[18]. Such calculation of the mean free path can be an underestimation, as the valence of Ti can change due to various reasons.

The mean free path can more accurately be approximated from AFM surface data where the average grain size can be obtained. An average of the height difference of the peaks and the valleys of the surface was used to approximate the half-width of the grain. This gives roughly results of 3 - 5 nm depending whether the wire is sputtered or not. The grain size value was calculated by measuring six areas of the wire from different positions and calculating the average value weighted by the size of each projected area. The results for non-sputtered wire grain diameter $W_{non-sput} = 5.1$ nm and for sputtered sample $W_{sput} = 3.1$ nm. The sputtered sample was sputtered about 20 nm deep and the effect of the sputtering should be more or

less only shown on the surface layers which would mean that after such amount of sputtering the grain size shouldn't change even if the sample was to be sputtered more.

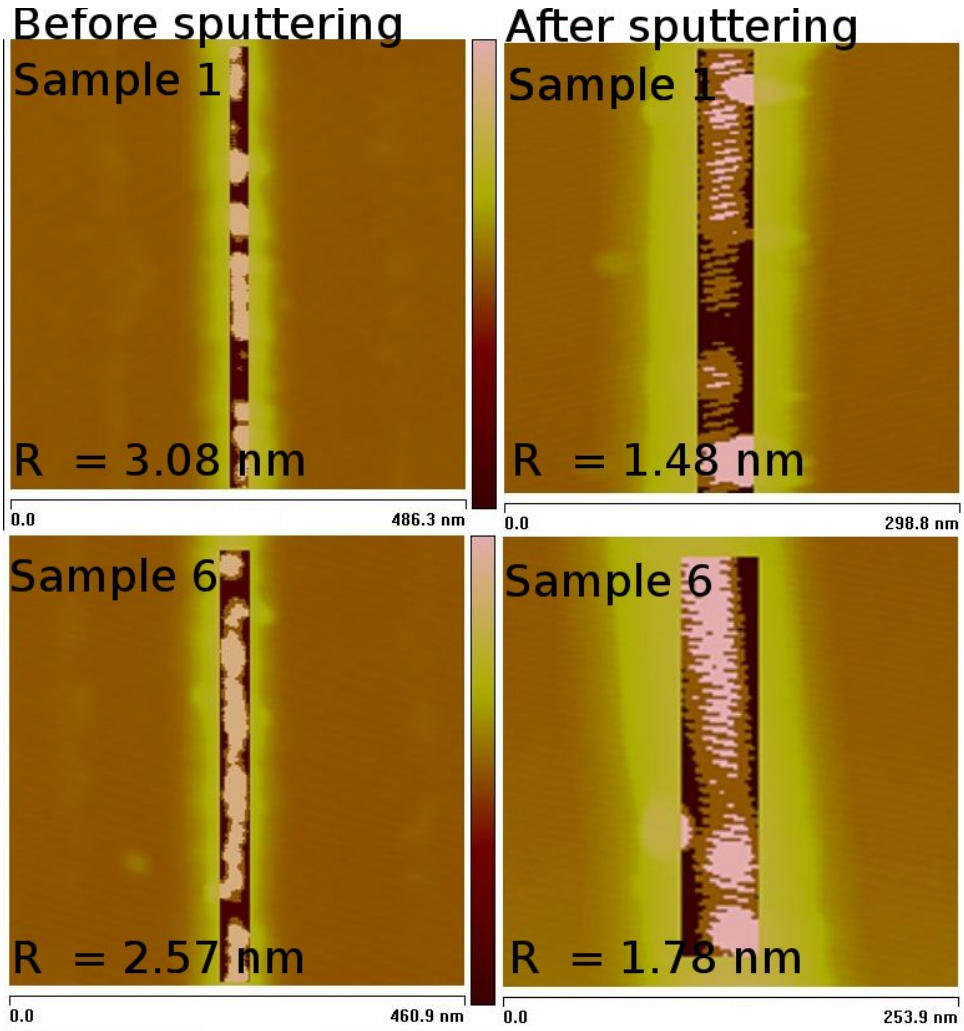

Figure 5.2: The AFM images of the wire parts where the roughness data have been taken. The surface of the projected area is set as zero plane and features smaller than 0.5 nm are neglected because that corresponds approximately the noise background of the AFM.

At first measurements only the R(T) transitions of the wire's were studied. The IVs of a nanowire with dimensions higher than QPS-regime wouldn't have given any extra information. The first IVs were taken when the nanowire was within sub-50 nm regime. The IVs were taken in different temperatures ranging from normal state

to deep within superconducting state in order to verify that the wire behaves as predictions dictate and possible junctions or Coulomb blockades could be found.

The temperature depence of the critical current was compared to the theoretical dependancy and was verified to be within reasonable limits with the theory $\propto (1 - T/T_c)^{3/2} = (1 - t)^{3/2}$. The theory should give good results only near T_c which for the wire was around 287 mK. The results seem to be quite well within the theory even well below T_c. The IVs of a nanowire with dimensions approximately 35 nm and the temperature depency of the critical currents is presented in Figure 5.3.

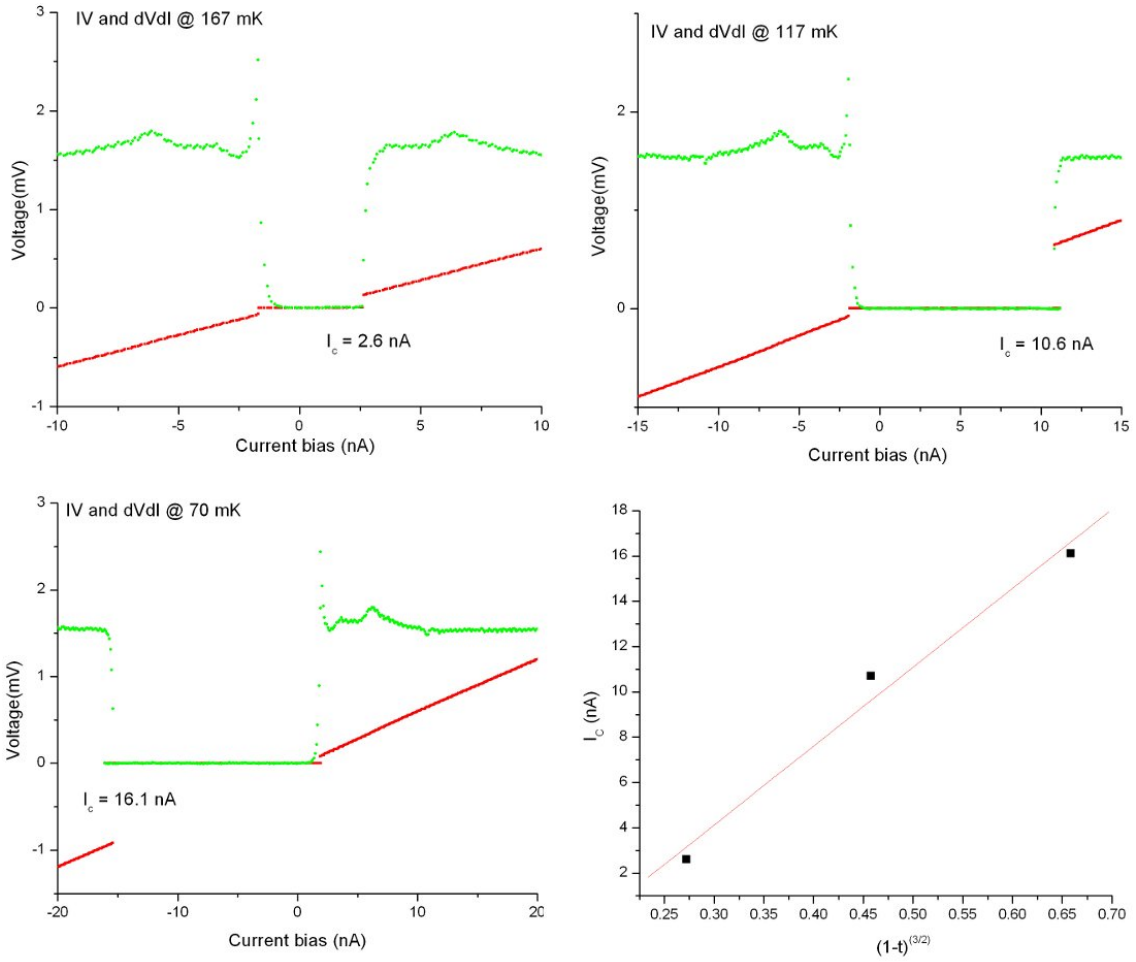

Figure 5.3: The IV-curves of a nanowire with dimensions approximately 35 nm in different temperatures. The critical currents as a function of temperature dependancy are plotted which should result in linear behaviour.

The wire diameters based on the resistances of the wires were between 29 nm

and 58 nm. This estimation for the wire's dimensions give too small results since the resistivity of the sputtered wire is higher due to the smaller average grain size. The more precise measurement of dimensions of the wire will be done after some sputtering cycles but for the moment the fact that the wire's dimensions are atleast three times higher than in any nanowire which has been measured to show QPS-behaviour. The uniformity of the wire will be easy to measure in such nanowire compared to the earlier measured aluminium nanowires which had dimensions below 10 nm.

The IVs of the wires were taken with high accuracy after the last sputtering session. The first IVs were taken in temperatures where the wire is in normal state. The temperature was chocen to be 1.2 K which is stable since that temperature can be reached just by pumping ^{4}He. These measurements were made to verify that the wire's wouldn't have any coulomb blockades. The graphs of the IVs are presented in Figure 5.4.

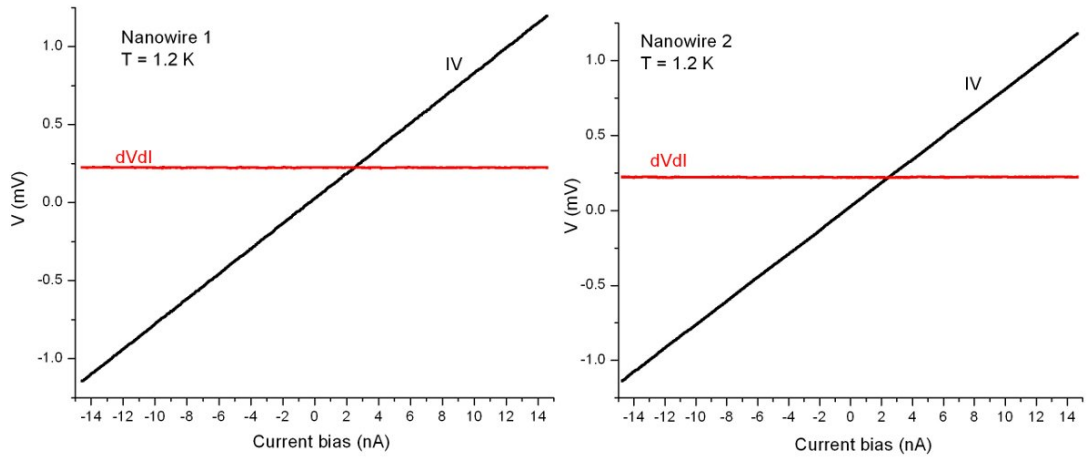

Figure 5.4: IV- and dV/dI-curves of the narrowest titanium nanowires using lock-in technique and small AC current on top of the DC-bias. No signature of the Coulomb blockade was detected.

5.1.2 Observation of the QPS phenomina

The QPS-phenomina was predicted to dominate the transition of the titanium nanowires with dimensions 35 nm and below. The high resistivity companied with low transition temperature are the key factors why titanium has promising properties for observations of QPS. The measurement of titanium samples needs low temperatures as the transition temperature is low. Those temperatures are still avalable by using dilution refrigerator.

The sample was measured five times. The first measurement was made when the wire was as fabricated. The later measurements were made after different sputtering dosages. The wire's dimensions were reduced from 59 nm to approximately 29 nm. The dimensions of the original wire were first measured by SEM and AFM and the resisitivity of the wire calculated based on those and four-probe resistance measurements. The cross-sections of the sputtered wires were calculated using this resistivity value.

The main part of the experiment was to measure the resistances as a function of the temperature for nanowires of different dimensions. The resistances were measured using small AC-currents and lock-in technique. The transitions are compared to the predictions of QPS-model and LAHM-model. In Figures 5.5 and 5.6 the transition curves of the nanowires are plotted with the predictions of the theoretical models. The QPS-fitting parameters are listed in table 5.1 and parameters for LAHM-model in table 5.2.

The QPS-fits were made using equation 3.50. This simplified formula gave good approximation for the transition in about two decade regime, depending the wire's dimensions. The fit is valid only in the regime well below the transition temperature. To attain reasonable fits the fitted transition temperatures were at lower values than the real transition temperature. Yet explanation for this is unknown but most probably it is due to model's limitations or the energy gap's temperature dependency is more complex than the calculated model. The fits worked better for the second nanowire which could indicate that the second wire was more uniform and as such doesn't have local variation of the transition temperature.

Nanowire 1 - QPS fits					
Cross-section(nm)	$R_N(\Omega)$	A	T_C(K)	S_{QPS}(T=0)	ξ_{eff}(T=0)(nm)
58	19350	0.230	0.335	10.21	148
53	23100	0.270	0.300	9.46	157
50	26600	0.315	0.291	9.46	159
33	53000	0.580	0.240	7.77	179
29	80400	0.610	0.142	4.23	228
Nanowire 2 - QPS fits					
Cross-section(nm)	$R_N(\Omega)$	A	T_c(K)	S_{QPS}(T=0)	ξ_{eff}(T=0)(nm))
58	19750	0.255	0.349	11.32	145
53	23850	0.310	0.326	10.8	153
48	28500	0.370	0.282	10.19	162
35	60000	0.760	0.192	8.34	193
29	76000	0.710	0.135	5.10	233
Mean-free-path 3.0 nm Fermi velocity 1.79 $*10^6$ m/s					

Table 5.1: Parameters of the QPS-fits of the nanowire 1 and nanowire 2. The corresponding plots are in Figure 5.5 and Figure 5.6. Cross-section is only used to identification not as parameter. The fit parameters are A and T_c. Normal state resistance is measured by four-probe DC-measurement and ξ calculated by BCS expressions and using the modified expression for the temperature 3.20 and taking the effective maximum. The equation is valid only in the range $1/4T_c - T_c$ and would give underestimated value for $\xi(T = 0)$.

Nanowire 1 - LAHM fits			
Cross-section(nm)	T_c(K)	B_c(mT)	ξ(T=0)(nm)
58	0.4	2.35	136
35	0.31	1.50	154
Nanowire 2 - LAHM fits			
Cross-section(nm)	T_c(K)	B_c(mT)	ξ(T=0)(nm)
58	0.4	2.35	136
33	0.27	1.00	158
Mean-free-path 3.0 nm Fermi velocity 1.79 $*10^6$ m/s			

Table 5.2: Parameters for LAHM-fits. The corresponding plots are in Figure 5.5 and Figure 5.6. The critical magnetic field is used as fitting parameter. The critical magnetic field for the wires is verified experimentally to be over 10 mT. The lower critical magnetic field rounds the theoretical transition curve by lowering the saddlepoint potential F_0.

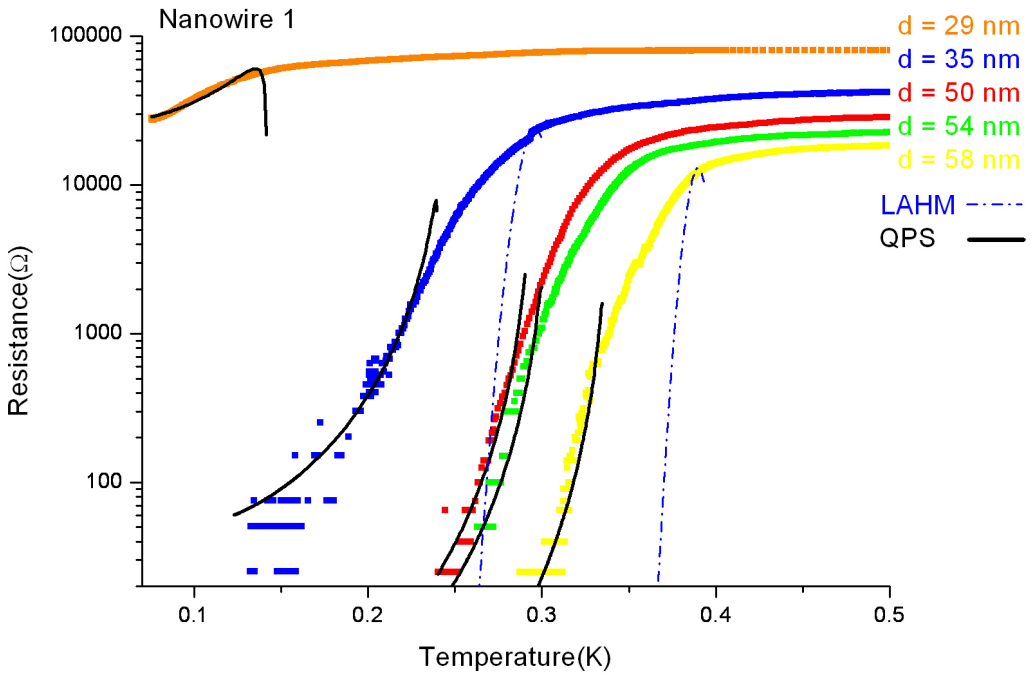

Figure 5.5: Experimental data and the theoretical fits for nanowire 1. The parameters for theoretical fittings are in table 5.1 and in table 5.2.

The LAHM-model gives dramatic discrepancy with the experimental data utilizing reasonable parameters. In the fits the critical magnetic field is underestimated for to have the absolute value of the resistance at right height. This rounds the transition but still the model gives transition which even at the case of the unsputtered wire is far sharper than in the experimental data. This is a clear indication that the LAHM-model is not able to explain the transition even of titanium nanowire with diameters 60 x 57 nm.

The proof of several IV and VI sweeps indicate that there are no other anormalities in the wires such as Coulomb blockades. The wires were imaged at detail when as fabricated and were of high uniformity. The wire's transition curves indicate that wire's are of good uniformity after the sputtering. It can be concluded that the model which better describes the behaviour of the nanowire's at diameters below 60 nm is the QPS-model. More theoretical calculations are needed in order to have

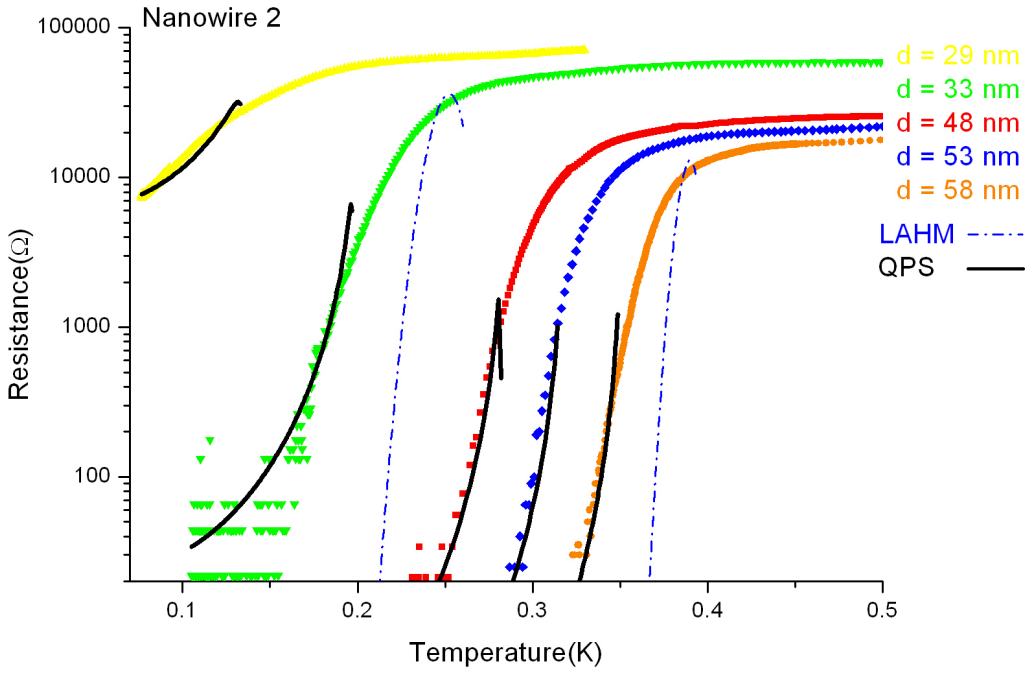

Figure 5.6: Experimental data and the theoretical fits for nanowire 2. The parameters for theoretical fittings are in table 5.1 and in table 5.2.

the model work in broader range. LAHM-model was found to be unable to explain to behaviour of the wires.

5.2 Titanium wire in highly resistive environment

The measurement of the sample consisted of two parts. First the properties of the resistive probes were measured. Titanium is highly resistive metal in normal state and thus short highly resistive wires can be fabricated out of it if the superconductivity can suppressed. The IV-characteristics should be linear which confirms that there are junctions between the titanium layers. The measured part of the resistor wire was 1.8 μm long. The wires were measured from the both sides of the sample. In the Figure 5.7 is IV characteristics of single probe at 70 mK measured in 4-probe configuration with AC modulation.

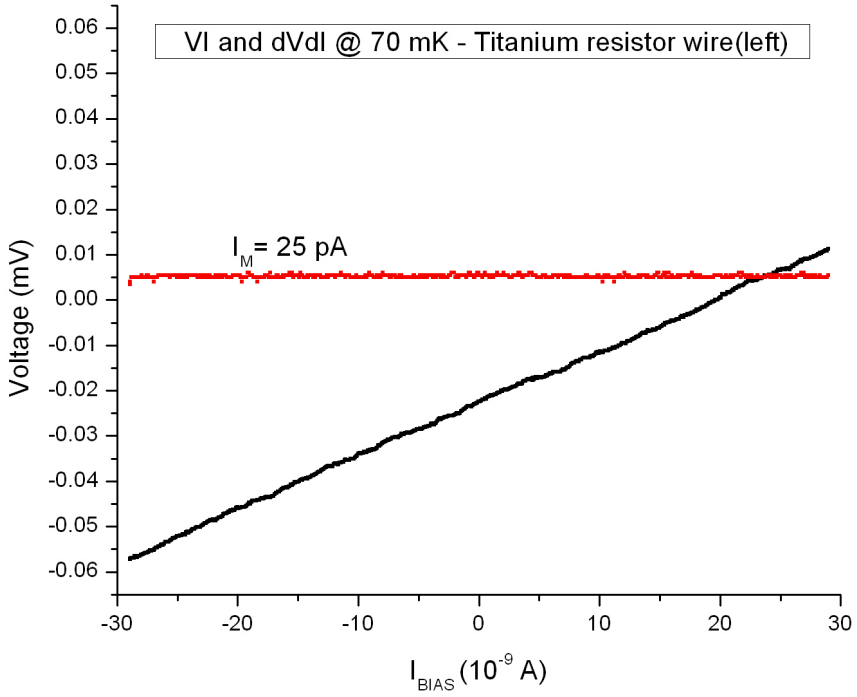

Figure 5.7: IV and dIdV of a "dirty" titanium nanowire well below expected transition temperature for the "clean" rival. The wire's cross section on the measured area is about 100 nm x 45 nm.

The resistance calculated from the DC-measurement IV at 70 mK is 1170 $\pm$ 3 Ω which is reasonable for such wire. The resistivity is approximately 586 $\mu\Omega\ cm$ at 70

mK. The literature values for bulk commercial grade titanium is about $10-15\ \mu\Omega\ cm$ at 77K [17].

The cross section of the resistive wires closer to the superconducting wire is much smaller making the resistance of the probe higher on those parts. The probes can be seen from the Figure 5.8. Left probe is meant for the current bias and the left one is for voltage measurement when measuring the long superconducting wire and the two probes coming from left to the resistivive probe are used to measure voltage over the resistive probe.

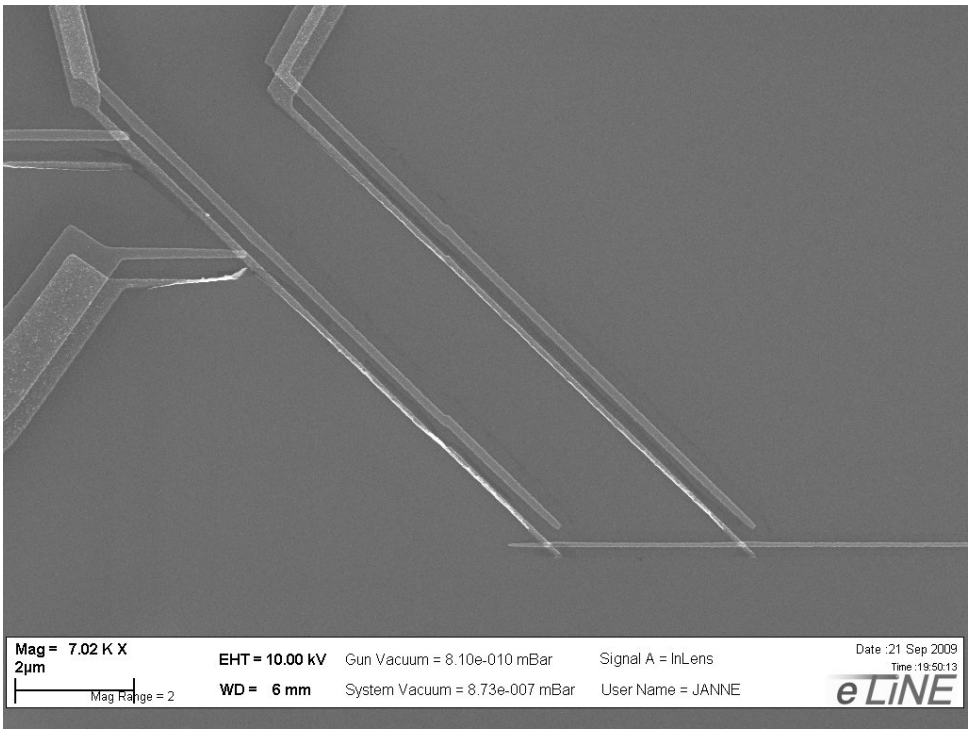

Figure 5.8: A SEM image of the resistor probes made out of dirty titanium.

As it can be seen from the IV-characteristics the resistive probe didn't have superconducting properties at temperatures 70 mK. Still it needed to be verified that there where no temperature dependant behaviour on the larger part. In the Figure 5.9 the AC-measured resistance of the wire is ploted as a function of temperature.

The wire's resistance below 1 K didn't seem to have any kind temperature dependance. These results confirmed that the method of making the resistive probes out of dirty titanium works. The results were verified by measuring another resistive

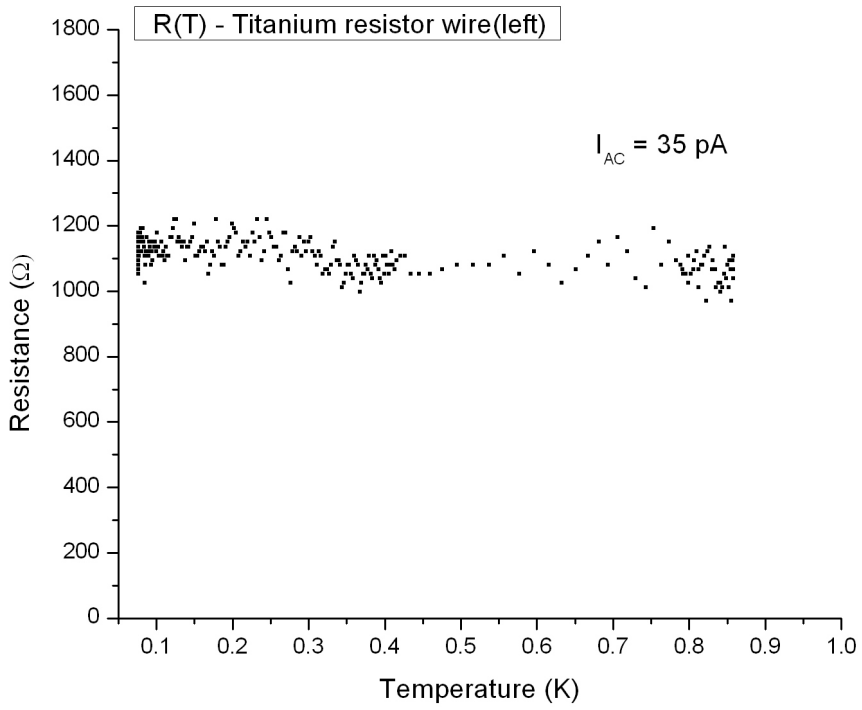

Figure 5.9: Temperature dependancy of the resistor probe measured by low frequency AC current and lock-in technique.

probe giving similiar results. The reproducability of this kind samples are yet to be tested but it seems likely since the sample worked as it was meant on the first try.

The other part of the measurement was to measure the long titanium wire. The wire's normal state resistance is about 85 $k\Omega$ which already means that it is about 14 times the R_q. The resistivity of the wire is 222 $\mu\Omega\ cm$ that is almost three times smaller than in the resistor lines. The wire is intresting to measure even at these dimensions as the normal state resistance is so high. The wire has superconducting transtion at approximately 260 mK. The transition is slightly curved at the lower resistance values and clearly transition width is several tens of millikelvins. The resistance as a function of temperature is presented in Figure 5.10.

The measurement had noise level of roughly 5 nV. The noise level could be reduced by using higher measurement current. In the other hand the higher current could cause some heating of the sample and distort the transition. The transition

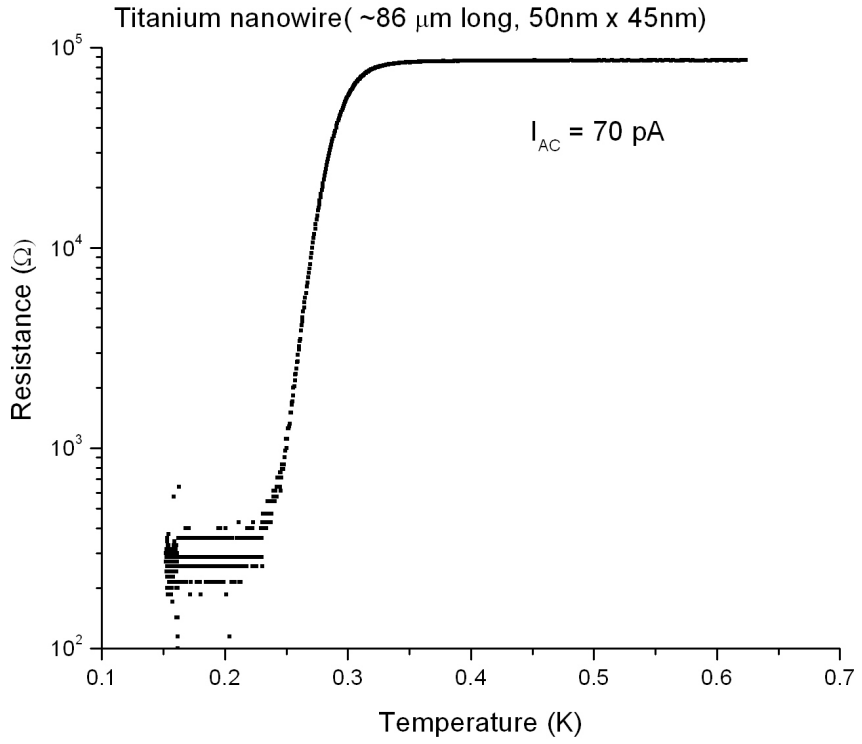

Figure 5.10: Superconductivity transition curve of a 85 μm long titanium nanowire within resistive environment with dimension approximately 50nm x 45 nm. The measurement was done with low frequency AC current and lock-in technique.

rounds to small residual residual resistance value which is still higher than the noise level would indicate. This is not likely to originate from QPS as the normal state resistor probes may cause small areas of the superconducting nanowire to go normal state by proximity effect and cause small, but measurable resistance.

The IV-measurements of the wire were made in temperatures 110 mK, 135 mK, 240 mK and 1.1 K. The IVs with dV/dIs are presented in Figure 5.11. The resistance calculated from the DC-measurement at 135 mK which is well below the transition temperature gives resistance value 100 $\pm$ 100 Ω. There might be some additional noise in the DC-measurement because of the modulation signal. In the Figure 5.12 the DC-points of the IV-curve at 135 mK are ploted in the range of roughly $-0.5 - 0.5\ nA$ and a linear fit made to determine the DC-measured resistance in

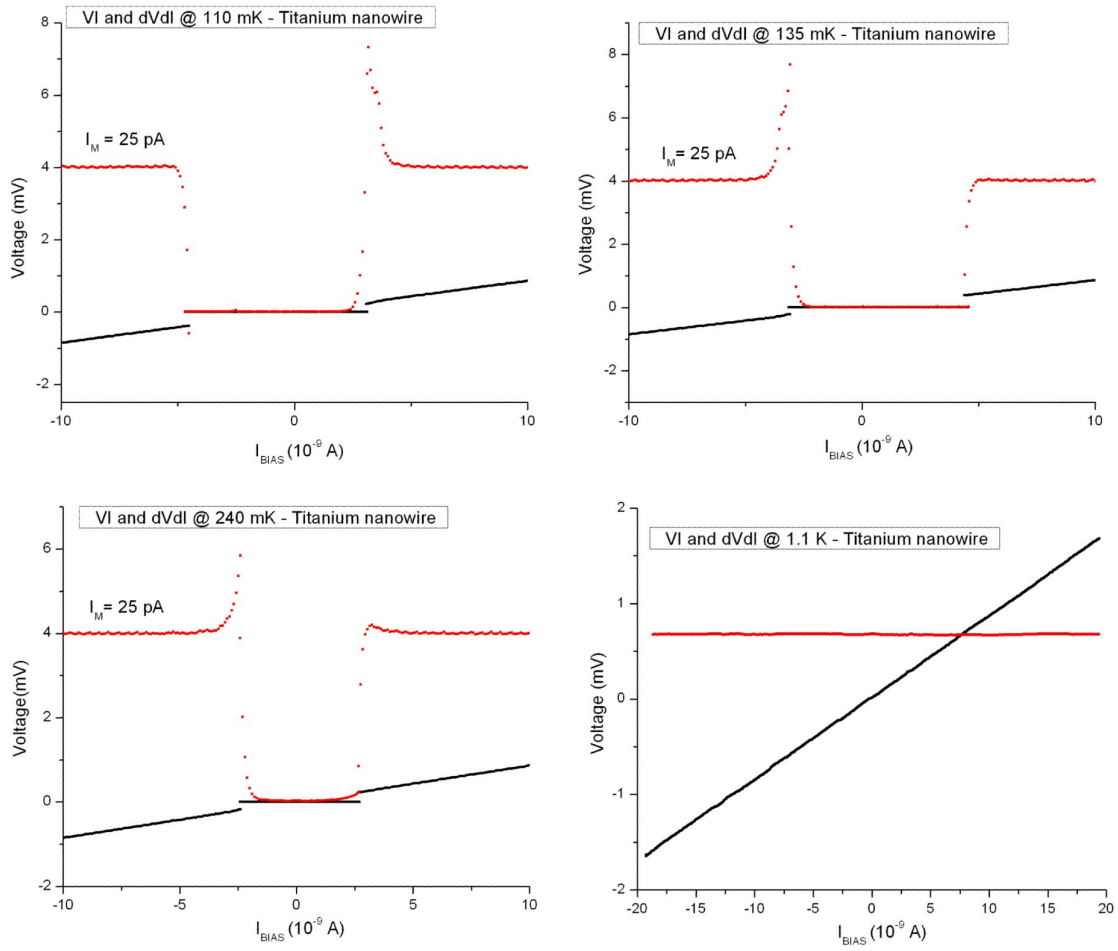

Figure 5.11: IV and dIdV measured in four different temperatures. The black lines are the IVs and red ones are the dIdVs.

the superconducting state.

The results are very promising and the behavior of the nanowire in all aspects seem to be well within predictions of the theory. The quantum fluctuations should be observable after some reduction of the dimensions. The method for fabrication is more than promising and can be used make the structres for experimental research of the phase-slip junction theory.

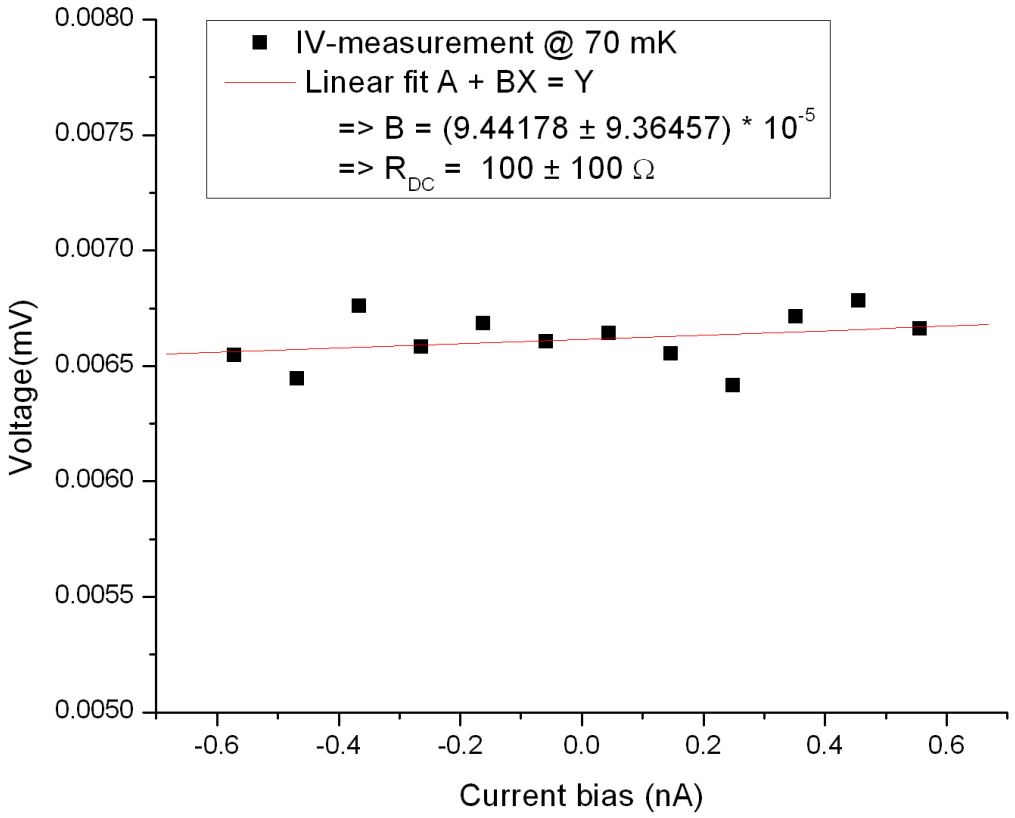

Figure 5.12: The IV of the long nanowire at 135 mK. The linear fit is made to calculate the resistance.

Chapter 6

Conclusions

Electron beam lithography, reactive ion etching and UHV metal evaporation was utilized to manufacture high purity uniform polycrystalline titanium nanowires. Properties of titanium were utilized to develop a fabrication method for making high resistance environment NSN structures out of titanium. The fabrication methods include only standard cleanroom equipment and should be easily reproducable.

The experiment showed that the theory for thermally activated phase-slips can't be used to explain superconducting transition of narrow titanium nanowires. On the other hand the theory for the quantum phase slips was successfully used to describe the lower region of the transition. The model for the QPS could fit the low-T end of R(T) transitions in wires with diameters up to 58 nm. The samples showed QPS-behaviour even when those were as-fabricated.

The uniformity of the wires is verified by AFM and SEM measurements when the wire was as fabricated. The transitions of the sputtered wire correspond the theoretical behaviour and low energy Ar^+ sputtering was used succesfully to reduce dimensions of the nanowires between the measuring sessions. The method is tested to be non-destructive and has been used for manufactoring uniform nanowires down to 10 nm.

The studies were made with the same wires progressively reducing the dimensions of the wires which enabled to observation of gradual crossover between superconducting and quasi-normal, quantum phase-slip dominated regime. The crossover

between the regimes is very sharp and change of few nanometers of the wire cross-section determines the wether the wire has superconducting state.

A leap towards making the Quantum Mechanical Standard for the current was made. The high resistive normal state titanium with suppressed superconductivity as resistive probe material and high quality titanium as superconducting material seem to be quite ideal candidates for structure in which the phase-slip junctions could be observed. There are many challenges still to face but the results are promising. The presented study is also significant for setting the fundamental limitations for miniaturization of superconducting elements in electronic nanocircuits. It shows that QPS behaviour can be expected within wires of relativly high dimensions. It also gives limits for producing quasi-normal state titanium nanowires as building block for quantum bits.

Bibliography

[1] J. Bardeen, L. N. Cooper, J. R. Schrieffer, *Theory of Superconductivity*, Phys. Rev. **108**, 1957.

[2] W. A. Little, *Decay of persistent currents in Small superconductors*, Phys. Rev. **156**, 1967.

[3] Michael Tinkham, *Introduction to superconductivity second edition*, Dover publications INC, N.Y., 2004.

[4] J. S. Langer, V. Ambegaokar, *Instrisic Resistive Transition in Narrow Superconducting Channels*, Phys. Rev. **164**, 1967.

[5] D. E. McCumber, *Instrisic Resistive Transition in Thin Superconducting Wires Driven from Current Sources*, Phys. Rev. **172**, 1968.

[6] D. E. McCumber, B.I Halperin *Time Scale of Intrinsic Resistive Fluctuations in Thin Superconducting Wires*, Phys. Rev. **B1** 1054, 1970.

[7] J. E. Lukens, R. J. Warburton, W. W. Webb *Onset of Quantized Thermal Fluctuations in "One-Dimensional" Superconductors*, Phys. Rev. Lett. **25**, 1970.

[8] R. S. Newbower, M. R. Beasley, M. Tinkham *Fluctuation Effects on the Superconducting Transition of Tin Whisker Crystals*, Phys. Rev. **B5** 864, 1972.

[9] N. Giodano, *Superconducting Fluctuations in One Dimension*, Physica B **203** 460, 1994.

[10] J. Duan, *Quantum Decay of One-Dimensional Supercurrent: Role of Electromagnetic* Field Phys. Rev. Lett. **74**, 1995.

[11] A. D. Zaikin, D. S. Golubev, A. von Otterlo, G. T. Zimanyi, *Quantum Phase Slips and Transport in Ultrathin Superconducting Wires*, Phys. Rev. Lett. **78**, 1997.

[12] K. Yu. Arutyunov, D. S. Golubev, A. Zaikin, *Superconductivity in one dimension*, Phys Rep. **469**, 1 (2008).

[13] M. Zgirski, *Experimental study of fluctuations in ultra narrow nanowires*, Academic Dissertation for Degree of Doctor of Philisophy, University of Jyväskylä, 2008.

[14] J.E. Mooij, G. Schön, *Propagating Plasmon mode in Thin Superconducting Filaments*, Phys. Rev. Lett. **55**, 1985.

[15] M. Zgirski, K-P Riikkonen, V. Tuboltsevm P. Jalkanen, T.T. Hongisto, K. Yu. Arutyunov, *Ion beam shaping and downsizing of nanostructures*, Nanotechnology **19**, 2008.

[16] J.P. Pekola, J.P. Kauppinen, *Insertable dilution refridgerator for characterization of mesoscopic smaples*, Cryogenics **34**(10), 1994.

[17] W. J. Lepkowski, J. W. Holladay, *The Physical Properties Of Titanium and Titanium Alloys*, TML Report No. **73**, 1957.

[18] Ashcroft, N. W. and Mermin, N. D., *Solid State Physics*, Saunders, 1976.

[19] Mika A. Sillanpää, Pertti J. Hakonen, *Titanium single-electron transistor fabricated by electron-beam lithography*, Physica E **15**, 2002.

[20] S. Tirelli, A. M. Savin, C. Pascual Garcia, J. P. Pekola, F. Beltram, and F. Giazotto, *Manipulation and Generation of Supercurrent in Out-of-Equilibrium Josephson Tunnel Nanojunctions*, Phys. Rev. Lett. **101**, 2008.

[21] Claire Dupas, Philippe Houdy, Marcel Lahmani, *Nanoscience*, Springer, Paris, 2006.